Amyloid beta induces the morphological neurodegenerative triad of spine loss, dendritic simplification, and neuritic dystrophies through calcineurin activation

Amyloid Beta (Aβ) Induces the Morphological Neurodegenerative Triad of Spine Loss, Dendritic Simplification, and Neuritic Dystrophies through Calcineurin (CaN) Activation

Hai-Yan Wu[1], **Eloise Hudry**[1], **Tadafumi Hashimoto**[1], **Kishore Kuchibhotla**[1,2], **Anete Rozkalne**[1], **Zhanyun Fan**[1], **Tara Spires-Jones**[1], **Hong Xie**[1], **Michal Arbel-Ornath**[1], **Cynthia L. Grosskreutz**[3], **Brian J. Bacskai**[1], and **Bradley T Hyman**[1]

[1]Massachusetts General Hospital, Department of Neurology/Alzheimer's Disease Research Laboratory, 114 16th Street, Charlestown, MA, 02129, USA

[2]Program in Biophysics, Harvard University, Cambridge, MA, 02138, USA

[3]Department of Ophthalmology, Massachusetts Eye and Ear Infirmary, 243 Charles Street Boston, MA, 02114, USA

Abstract

Amyloid beta containing plaques are surrounded by dystrophic neurites in the Alzheimer disease (AD) brain, but whether and how plaques induce these neuritic abnormalities remain unknown. We tested the hypothesis that soluble oligomeric assemblies of Aβ, which surround plaques, induce calcium mediated secondary cascades that lead to dystrophic changes in local neurites. We show that soluble Aβ oligomers lead to activation of the calcium-dependent phosphatase CaN (PP2B) which in turn activates the transcriptional factor nuclear factor of activated T cells (NFAT). Activation of these signaling pathways, even in the absence of Aβ, is sufficient to produce a virtual phenocopy of Aβ induced dystrophic neurites, dendritic simplification, and dendritic spine loss in both neurons in culture and in the adult mouse brain. Importantly, the morphological deficits in the vicinity of Aβ deposits in a mouse model of AD are ameliorated by CaN inhibition, supporting the hypothesis that CaN/NFAT are aberrantly activated by Aβ, and that CaN/NFAT activation is responsible for disruption of neuronal structure near plaques. In accord with this, we also detect increased levels of an active form of CaN and NFATc4 in the nuclear fraction from the cortex of patients with AD. Thus, Aβ appears to mediate the neurodegeneration of AD, at least in part, by activation of CaN and subsequent NFAT-mediated downstream cascades.

Keywords

Calcineurin; NFAT; Amyloid Beta; Morphological changes; Neurodegeneration; Alzheimer; synaptic dysfunction

Introduction

Aβ peptide, the major component of senile plaques, accumulates in the brain of AD patients (Walsh and Selkoe, 2004; Yaari and Corey-Bloom, 2007). The amyloid hypothesis (Hardy and Allsop, 1991; Hardy and Selkoe, 2002) suggests that Aβ induces neurodegeneration, but the

key molecular mechanisms that link Aβ to neuronal damage remain a critical gap in understanding AD and designing effective therapeutics. Exposure of neurons to synthetic or naturally secreted Aβ peptides induces a reduction of dendritic spines and synaptic dysfunction in culture, and causes memory deficits in learned behavior in normal rats (Pike et al., 1993; Lorenzo and Yankner, 1994; Geula et al., 1998; Shankar et al., 2007; Shankar et al., 2008). *In vivo* studies using longitudinal multiphoton microscopy reveal a direct toxic effect on neurites surrounding Aβ deposits, including dendritic simplification, loss of dendritic spines, and neuritic dystrophies (Spires et al., 2005; Meyer-Luehmann et al., 2008). However, the connection between extracellular Aβ and the intracellular signaling pathways that cause local disruption of neuronal processes, synaptic dysfunction, and neurodegeneration are unknown.

Elevated intracellular calcium has been observed in neurons exposed to Aβ in several model systems and disrupted calcium homeostasis has been suggested to play a central role in AD pathogenesis (Palotas et al., 2002; Mattson, 2004; Smith et al., 2005; Stutzmann, 2005; Bezprozvanny and Mattson, 2008; Busche et al., 2008). For example, we have recently demonstrated that neurites in APP overexpressing transgenic mice have significantly elevated intracellular calcium ($[Ca^{2+}]i$) compared to age-matched nontransgenic controls (Kuchibhotla et al., 2008).

In neurons, Ca^{2+} signaling is tightly controlled to ensure proper functioning of numerous Ca^{2+}-dependent events including processes influenced by the serine/threonine phosphatase CaN (Mulkey et al., 1994; Wang and Kelly, 1996; Halpain et al., 1998; Berridge et al., 2000). CaN is the only Ca^{2+}-activated protein phosphatase in neurons and it is involved in many facets of neuronal physiology, including synaptic plasticity, and learning and memory (Klee et al., 1979; Winder and Sweatt, 2001). In mice, both genetic and pharmacological upregulation of the expression of CaN can induce synaptic dysfunction and memory impairment, while CaN inhibition strengthens memory in spatial learning tasks (Malleret et al., 2001; Winder and Sweatt, 2001; Mansuy, 2003). We explored the possibility that AD-related neuritic degeneration may involve altered CaN activity as a result of Ca^{2+} dyshomeostasis.

In the present study, we establish an *in vitro* model of Aβ-induced neuritic damage. Using this model, we established molecular links between exposure to extracellular Aβ and the morphological changes that occur in neurites around plaques. We find that soluble Aβ from Tg2576 conditioned medium (CM) induces CaN activation and subsequent NFATc4 nuclear translocation, which leads to dendritic spine loss, dendritic simplification, and neuritic dystrophies. Blocking Aβ, CaN activation, or importantly, NFAT activation is each sufficient to prevent Aβ-induced morphological alterations. Moreover, plaque-associated neurodegenerative changes in an APP overexpressing mouse model of AD can be blocked by inhibiting CaN. These data suggest that CaN activation and subsequent activation of NFAT-mediated transcriptional cascades are critically involved in Aβ-induced neurotoxicity, providing mechanistic insight into the "black box" between Aβ and synaptic failure.

Materials and Methods

Primary Neuronal Cultures

The animals utilized for generating cell cultures were transgenic mice expressing human APP (Tg2576 line: transgenic mice overexpressing the 695-amino acid isoform of human Alzheimer β-amyloid precursor protein containing the double Swedish mutation K670N, M671L with a hamster prion protein gene promoter in B6;SJL F2 mice) (Hsiao et al., 1996). Primary neuronal cultures were derived from cerebral cortex of embryonic day (E) 15–19 Tg2576 mice (Charles River Laboratories, MA), as described previously (Wu et al., 2004) with modifications. Briefly, cortices were dissected, gently minced, trypsinized (0.027%, 37 °C; 5% CO_2 for 15 min), and then washed with 1×HBSS. Neurons were seeded to a density of 4×10^5 viable cells/35-mm

culture dishes previously coated with poly-D-lysine (100 µg/ml) for at least 1 hour at 37 °C. Cultures were maintained at 37 °C with 5% CO_2, supplemented with neurobasal medium with 2% B27 nutrient, 2 mM L-glutamine, penicillin (100 units/ml) and streptomycin (100 µg/ml). The cultures were used within 28 DIV. To maintain elevated levels of extracellular Aβ, media was not changed. To identify the genotype of the animals, we used the polymerase chain reaction on DNA extracted from sample tail taken after dissection of the cerebral cortex.

Adeno-associated Viral (AAV) Construction

AAV with an expression cassette of the chicken β-actin promoter driving EGFP or CaNwt or CaNCA or AKAP79 peptide, flanked by the AAV ITRs, was described previously (Spires et al., 2005). The mouse CaN isoform cDNA corresponding to wild-type (CaNwt), CaNCA (amino acid residues 1–399), and a peptide corresponding to human AKAP79 (hAKAP79, amino acid residues 60–358) were subcloned into AAV-CMV/CBA-WPRE vector. Each construct was amplified by the following primers : (1) H A-CaNwt-V 5 5 ' , GAATTCATGTATCCGTATGACGTACCAGAGTACGCCATGTCCGAGCCCAAGG CGATTGATCC; (2) HA-CaNwt-V 5 3 ' , GCTAGCTCACGTACTGTCGAGTCCCAGGAGAGGGTTTGGGATCGGCTTGCCC TGGATATTGCTGCTATTACTGCCATTGC; (3) HA-C a N C A 3 ' , CTAGTTCTGATGACTTCCTTCCGGGCTGCGGCCGTC; (4) Flag-hAKAP79 5' GAAGTTATCAGTCGACATGGACTACAAAGACGATGACGACAAGGGCAGGAA GTGTCCACAA; (5) Flag-h A K A P 7 9 3 ' , ATGGTCTAGAAAGCTTCTAGACATTTTTAGATTTTGTAACATCAAATTCACTG ATTTC. All the constructs were verified by sequencing.

Immunocytochemistry

Immunocytochemistry was performed as described previously (Wu et al., 2004). Briefly, after being treated under different experimental conditions, cells were fixed with 4% paraformaldehyde in phosphate-buffered saline (PBS) (pH 7.4) for 15 min and were then membrane-permeabilized with 0.5% Triton X-100 in PBS for 5 min. After blocking with 3% bovine serum albumin at 37 °C for 1 h, cells were incubated with primary antibodies: anti-microtubule-associated protein 2 (MAP2) antibody (1:200, Sigma), or anti-NFATc4 antibody (1:200, Santa Cruz), anti-HA antibody (1:200, Molecular Probes), or anti-flag antibody (1:200, Sigma), at 4 °C overnight. Cells were then incubated with secondary antibodies conjugated to either cyanine 3 (Cy3, 1:500; Jackson ImmunoResearch), or Alexa 488 (1:500; Molecular Probes). Fluorescent images were obtained using a LSM 510 Zeiss microscope with a 25 × or a 63 × water-imersion objective lens. All images were taken at 512 × 512 pixel resolution. Nuclear NFATc4 staining was determined by overlap of NFATc4 staining with Hoechst nuclear staining. To calculate the NFATc4 ratio of nucleus vs cytoplasm, the intensity of nuclear NFATc4 was divided by the intensity of cytoplasmic NFATc4.

Immunohistochemistry

Immunohistochemistry was performed as described previously (Spires et al., 2005). Briefly, animals were killed with an overdose of Ketamine (30 mg/kg) and Xylazine (3 mg/kg), and the brain was fixed in 4% paraformaldehyde in phosphate buffer with 15% glycerol cryoprotectant. Sections of 100 µm were cut on a freezing microtome, washed extensively in 0.1 M phosphate buffer and processed as free-floating slices. Permeabilization and blocking was achieved by incubation of the sections for 1 h at room temperature in 0.1 M phosphate buffer, 0.5% Triton X-100 (vol/vol) and 3% bovine serum albumin. Primary antibodies for GFP (1:1000, Biogenesis), HA (1:100, Molecular Probes), Flag (1:100, Sigma), SMI312 (1:200; Sternberger Monoclonals) were applied overnight at 4 °C in 0.1 M phosphate buffer with 3% bovine serum albumin. Following extensive washing, appropriate secondary

antibodies conjugated to either Cy3 (1:100 dilution), Alexa 488 (1:100 dilution) or Cy5 (1:100 dilution) were applied for 1 hour at room temperature. Micrographs of immunostaining were obtained using a $20 \times$ objective with an upright Olympus Optical BX51 fluorescence microscope with an Olympus Optical DP70 camera, or using a $63 \times$ water-immersion objective with a Zeiss confocal microscope.

Preparation of Subcellular Fractionation

Frozen tissue samples of human brain cortex (250 mg) were homogenized in 0.32 M sucrose lysis buffer (0.32 M sucrose, 5 mM $CaCl_2$, 3 mM Mg(Acetate)$_2$, 0.1 mM EDTA, 10 mM Tris-HCl (pH 8.0) and 0.1% Triton X-100), supplemented with complete protease inhibitor cocktail tablets and centrifuged at $800 \times g$ for 15 min at 4 degrees. The supernatants were centrifuged at $100,000 \times g$ for 1 hr at 4 degrees, and the resulting supernatants were regarded as the cytosolic fractions. The pellets from the initial centrifugation step were resuspended in 1.8 M sucrose buffer containing 1.8 M sucrose, 3 mM Mg(Acetate)$_2$, 1 mM DTT and 10 mM Tris-HCl (pH 8.0), supplemented with complete protease inhibitor cocktail tablets (Roche Diagnostics, IN, USA). The nuclei were pelleted by centrifugation at $12,400 \times g$ for 1 hr at 4 degree. The pellet was resuspended in 0.32 M sucrose buffer and washed by low-speed centrifugation. The final pellet was designated as the nuclear fraction.

For western blot analyses, equal amounts of protein (20 µg) from each fraction were separated on a 4–20% SDS-PAGE gel. Primary antibodies for CaN (Stressgen) and NFATc4 (Santa Cruz) were utilized. Primary antibody incubation was followed by rabbit polyclonal horseradish peroxidase linked secondary antibody (1:1000; Bio-Rad). Immunoreactivity was visualized using enhanced chemiluminescence reagent (Perkin-Elmar) and exposure on x-ray film. Anti-GAPDH antibody (Millipore) and anti-HDAC1 antibody (ABR-Affinity BioReagents) were used to verify the integrity of the cytoplasmic and nuclear fraction separation.

Separation of Aβ oligomers by size exclusion chromatography (SEC)

5 ml of cultured media from 14DIV wild-type or Tg neuron cultures was collected and centrifuged at $3,000 \times g$ at 4 degrees in Amicon Ultra-15ML 3K(Millipore) to concentrate proteins ~5 fold. 750 µl of concentrated cultured media was separated by SEC on Superdex 75 10/300 GL column (GE healthcare) in 50 mM ammonium acetate pH 8.5 with AKTA purifier 10 (GE healthcare) (Townsend et al., 2006).

ToxiLight BioAssay

Cell viability was determined in wild type or Tg neurons at both 7DIV and 14DIV using the ToxiLight BioAssay Kit from Lonza. Preparation of cell extracts and the cytotoxicity assay were performed according to the manufacture's protocol.

Aβ Assay

Aβ levels were assayed from the medium collected from culture dishes at different date, using an ELISA. Aβ concentration was determined with a sandwich ELISA kit (WAKO, Richmond, VA) and with BAN50/BA27 for Aβ40 and BAN50/BC05 for Aβ42 in cultured medium and with BNT77/BA27 for Aβ40 and BNT77/BC05 for Aβ42 in fractionated samples by size-exclusion chromatography. Samples was optimized to detect Aβ in the range of 6.25–100 fmol/ml. ELISA signals were reported as the mean ± SD of two replica wells in fmoles of Aβ per mg of protein (determined with the BCA Protein Assay Reagen Kit, Pierce).

Immunoprecipitation Aβ from Cultured Medium

Cultured medium of wild-type or Tg cultures at 14 DIV were collected. Medium was centrifuged at 1200 rpm for 5 min at 4 °C to remove cellular debris. Supernatants (1.3 ml) for

each condition were precleared with 50 µl protein G sepharose (Sigma) for 1 hour at 4 °C with gentle shake, then centrifuged at 15,000 rpm at 4°C for 5 min. Supernatants were incubated with 5 µg anti-6E10 antibody or 5 µg anti-GFP (Abcam) as control. After an overnight incubation at 4 °C, protein G sepharose (60 µl) were added and incubated at 4 °C for 2 h. Beads were isolated by centrifugation (15,000 rpm, 4°C for 5 min) and subsequently washed three times with TBS buffer before the addition of $2\times$ Laemmli sample buffer.

[Ca2+]i Measurements

Primary neurons were plated on 35 mm glass-bottom dishes (MatTek, Ashland MA) and maintained in a standard Neurobasal medium without Phenol Red. Calcium levels were evaluated in wild type neurons treated for 24 hours with wild type or Tg conditioned media as well as with transgenic conditioned media that was pre-depleted with 3D6 antibody. In all cases, calcium imaging was performed using Indo-1 as previously described(Bacskai et al., 2000). Briefly, Indo-1/AM (Molecular Probes) was dissolved with 20% pluronic F-127 (Molecular Probes) in DMSO and then added to the culture dishes at a final concentration of 1 µM Indo-1/AM and 0.02% pluronic F-127 for 45 min. Cells were imaged with an Olympus Fluoview 1000MPE with pre-chirp optics and a fast AOM mounted on an Olympues BX61WI upright microscope and an Olympus $20\times$ dipping objective (numerical aperture 0.95). A mode-locked titanium/sapphire laser (MaiTai; Spectra-Physics, Fremont, CA) generated two-photon fluorescence with 750nm excitation, and the emitted light was discriminated into two channels with interference filters corresponding to 390-nm, 65-nm band pass and 495-nm, 20-nm band pass (Chroma Technology, Brattleboro, VT) for ratiometric imaging. The capture settings remained unchanged for the entire experiment. Fluorescence emission ratios were calculated in the neuronal cell bodies. To convert the calculated ratios into calcium concentrations, primary neurons were incubated with Indo-1/AM and treated with either calcium free or 39µM calcium buffers in the presence of 20µM ionomycin for 15 min. The calcium free and calcium saturated ratios were then measured and used as the R_{min} and R_{max}. These ratio along with the K_D of Indo-1 for calcium of 250nM (Grynkiewicz et al., 1985) were used for calculation of calcium concentration.

Luciferase Reporter Assay

Mouse wild-type CaNA isoform (CaNwt), truncated CaNA encoding 45-kDa (CaNCA) isoform, or NFAT-TA-Luc (BD Biosciences Clontech), were subcloned into Adeno-associated virus (AAV serotype 2) vector. These plasmids (1 µg) were used primary neurons at 3 DIV. After 24 h, the cells were harvested and luciferase activities were measured with a luminometer using a reagent kit (Luciferase Assay System with Reporter Lysis Buffer, Promega). The background luciferase activity was subtracted from all experiments.

Experimental Animals

C57Bl/6J wild-type mice and double transgenic mice (B6C3APPswe/PS1dE9 line, Jackson laboratory) overexpressing mutant human APP and mutant human Presenilin 1, as well as transgenic mice expressing human Swedish mutated APP (Tg2576 line) were used. These mice were housed in the animal facility and C57Bl/6J wild-type and APP/PS1 mice were used at the age of 5–6 months for intracortical injection. All experiments were performed in accordance with animal protocols approved by the Institutional Animal Care and Use Committee.

Intracortical Injections and Surgery

Intracortical injections and surgery were performed as described previously (Spires et al., 2005; Kuchibhotla et al., 2008; Meyer-Luehmann et al., 2008). Briefly, mice were anesthetized with Ketamine (10 mg/kg) and Xylazine (1 mg/kg) and placed in a stereotaxic apparatus. The surgical site was sterilized with betadyne and isopropyl alcohol, and a 2–3 mm incision was

made in the scalp along the midline between the ears. Burr holes were drilled in the skull, 0.5 mm posterior from bregma and 0.5 mm lateral to the midsagital line. Using a Hamilton syringe, 3 µl of virus (titer, 4.2×10^{12} viral genomes/ml) was injected 1.2 mm deep in somatosensory cortex at a rate of 0.25 µl/min. After one injection in each burr hole, the scalp was sutured, and the mouse recovered from anesthesia on a heating pad.

3–4 weeks after injection, APP/PS1 transgenic mice received an intraperitoneal injection of methoxy-XO_4 (10 mg/kg), a fluorescent compound that crosses the blood-brain barrier and binds to amyloid plaques (Klunk et al., 2002). A cranial window of 6 mm in diameter was installed under anesthesia (Ketamine (10 mg/kg) and Xylazine (1 mg/kg)). At the same time, Texas Red dextran (70,000 Da molecular weight; 12.5 mg/ml in sterile PBS; Molecular Probes, Eugene, OR) was injected into a lateral tail vein to provide a fluorescent angiogram.

Multiphoton Imaging

Images of GFP-filled neuronal processes, and, in the case of APP/PS1 mice, amyloid pathology, and blood vessels were obtained using a Bio-Rad 1024ES multiphoton microscope (Bio-Rad), mounted on an Olympus Optical (Tokyo, Japan) BX50WI upright microscope. A wax ring was placed on the edges of the coverslip of the cortical window and filled with distilled water to create a well for an Olympus Optical 20× dipping objective (numerical aperture, 0.95). A mode-locked titanium/sapphire laser (MaiTai; Spectra-Physics, Fremont, CA) generated two-photon fluorescence with 800 nm excitation, and detectors containing three photomultiplier tubes (Hamamatsu, Ichinocho, Japan) collected emitted light in the range of 380–480, 500–540, and 560–650 nm (Bacskai et al., 2003). GFP-filled were sampled ~100 microns below the surface of the brain around somatosensory cortex. At the end of imaging sessions, mice were allowed to recover and placed singly in their home cage.

Labeling of Fibrillar Amyloid Deposits

Following immunohistochemistry, fibrillar amyloid deposits (neuritic plaques) were stained for 8 min in a solution of thioflavin S (2 µg/mL) in 0.1 M PBS and then rinsed with ddH_2O.

Statistical Analyses

Data are presented as mean ± standard deviation (SD). We made comparisons between groups by one- or two - way ANOVA followed by post-hoc Bonferroni's test for comparison among means. Differences with a *P* value of < 0.05 were considered statistically significant.

Results

Abnormal morphologies in neurons from Tg 2576 cultures

Neuritic abnormalities are seen surrounding plaques in human AD and in aged APP overexpressing mouse models of AD, but studying these lesions is difficult since they are distributed apparently randomly throughout the cortical mantle, occur only in aged animals, and the location of new lesions cannot be predicted. We sought to develop a tractable model for neuronal abnormalities associated with AD. We first examined whether mature primary neurons from transgenic embryos expressing APP with the familial Swedish (APP-SW) mutation (Tg 2576 line) develop any of the morphological phenotypes associated with neurodegeneration in the intact (aged) transgenic brain and in human AD including dendritic spine loss, diminished dendritic complexity, and neuritic dystrophies. To assess neuronal morphology, we transfected cultured neurons with green fluorescent protein (GFP) to label individual neurons. During the course of 21 days *in vitro* (DIV), GFP positive neurons from Tg 2576 (Tg) cultures progressively develop a neurodegenerative phenotype when compared to neurons from wild-type mice. In wild-type neurons at 14 DIV, GFP fluorescence

demonstrated intricately branched dendritic arbors studded with protrusions that included mature spines and few fillopodia (Fig. 1A1 and 1A3). However, in Tg neurons the maturation is accompanied by an increase in the number of neurons with focal neuritic swellings (Fig. 1A2 and 1A4). The difference is marked; for example, at 14 DIV (Fig. 1B), the number of neurons with beaded neurites in Tg cultures is 7-fold higher than those in wild-type cultures. In addition, the number of neurons with dystrophic neurites increased with time (Fig.1B). In Tg cultures, GFP-positive neurons with dystrophies are found in 14% of neurons at 14 DIV and in 24% at 21 DIV. Since some subtle morphological changes other than dendritic dystrophies, such as decreased dendritic branches and spine density, are also observed in the early stages of neurodegeneration, we next compared dendritic branching and the density of dendritic spines of GFP-positive neurons from Tg and wild-type cultures. As measured by Sholl analysis, neurons in Tg cultures had reduced dendritic complexity at all points farther than 30 µm from the cell body compared to wild-type cultures (Fig. 1C and D). These effects are not due solely to processes with overt morphological changes like dystrophies. For example, comparison of spine density in neurons (excluding neurons with dystrophies) between Tg and wild-type cultures showed that the mean spine density of Tg neurons is markedly lower than that of wild-type neurons (Fig. 1E and F). These effects are not due to overt toxicity; No typical apoptotic nuclei (chromatin condensation) appeared in Tg neurons compared with wild-type neurons (supplemental Fig. 1A). ToxiLight assay for cell death showed no significant difference between wild-type and Tg neurons at either 7 or 14DIV (supplemental Fig. 1B). Taken together, these results indicate that neurons with abnormal morphologies are limited in wild-type cultures, whereas in Tg cultures, neurons develop dystrophies, profound dendritic simplification, and loss of dendritic spines.

Conditioned media from Tg culture contains oligomeric Aβ and induces elevation of [Ca^{2+}]i

Primary cortical neurons derived from Tg embryos at 14 DIV produced high levels of two major types of human Aβ peptides, Aβ 40 and 42; the concentration of Aβ 40 was 16 ng/ml and of Aβ 42 was 1.2 ng/ml as determined by ELISA assay (supplemental Fig. 2A and B). Moreover, IP Western blot analysis revealed the presence of readily detectable SDS-stable small oligomers in CM of Tg cultures at 14 DIV, similar to those reported to be synaptotoxic (Shankar et al., 2008) (supplemental Fig. 2C).

We recently observed that neurites in the region near senile plaques contain high [Ca^{2+}]i (Kuchibhotla et al., 2008). To examine if Aβ is capable of inducing an increase in [Ca^{2+}]i, we studied the effect of Tg neuronal culture CM on calcium homeostasis of wild-type neurons. Wild-type cortical neurons were cultured in standard NB/B27-serum free medium and at 14 DIV, the medium was replaced with diluted 1:2 CM from wild-type or Tg cultures and further incubated for 24 hrs. As shown in supplemental Fig. 2D, wild-type neurons treated with Tg CM for 24 hrs exhibited elevated levels of [Ca^{2+}]i compared to neurons maintained in wild-type CM for 24 hrs. There was no significant difference in [Ca^{2+}]i levels between untreated neurons and neurons treated with wild-type CM (wtCM) for 24 hrs, indicating that the elevated levels of [Ca^{2+}]i specifically resulted from Tg CM. To determine if Aβ caused the elevation of the [Ca^{2+}]i, we compared [Ca^{2+}]i between neurons applying Tg CM with or without immunodepletion using 3D6 antibody, a high-titre monoclonal Aβ antibody (Johnson-Wood et al., 1997). 3D6 immunodepletion completely prevented the elevation of [Ca^{2+}]i (supplemental Fig. 2D).

CaN / NFATc4 - aberrant nuclear localization in neurons from Tg cultures and human AD postmortem brain

Since Aβ in Tg CM induces elevated [Ca^{2+}]i in cultured neurons, and our previous study showing that neurites with abnormal morphologies in both APP/PS1 and APP transgenic mice were strongly associated with [Ca^{2+}]i overload (Kuchibhotla et al., 2008), we examined

Ca^{2+} mediated pathways as the link between exposure to Aβ and a neurodegenerative phenotype. As CaN is the most calcium sensitive protein phosphatase in the brain (Klee et al., 1979), we examined whether CaN activity is upregulated in neurons from Tg cultures. NFATc4, the nuclear factor of activated T cells, is a well-known CaN substrate. Activation of the predominant neuronal NFATc4 isoform, which is abundantly expressed in cortical neurons, can be determined by its nuclear translocation following CaN-mediated dephosphorylation. Cultured neurons were stained with an antibody against endogenous NFATc4, a Hoechst counterstain for identification of nuclei, and MAP2, a neuron marker (Fig. 2A). The NFATc4 immunofluorescence intensity was measured and the ratio of the intensity (nucleus vs cytoplasm) was compared in neurons from wild-type and Tg cultures. Very little colocalization of Hoechst nuclear staining and NFATc4 was found in wild-type neuron cultures, indicating that inactive NFATc4 is mostly located in the cytoplasm, whereas in Tg culture, NFATc4 staining was enhanced in nuclei (Fig. 2A and B). Similarly, CaN is known to translocate to the nucleus when activated, and Tg neuron cultures showed higher immunofluorescence intensity of CaN in the nucleus compared to wild-type neurons (Fig. 2C and D). These data show that CaN and NFAT are activated in Tg neurons.

To determine whether the aberrant nuclear localization of CaN / NFATc4 observed in Tg neurons could be relevant to the AD human condition, total homogenates, cytosol, and nuclei were prepared from frozen human AD or control cortex tissue samples and analyzed by immunoblotting with antibodies against endogenous NFATc4 or CaN (supplemental table 1 and Fig. 2). NFATc4 immunoreactivity in the nuclear fraction prepared from AD samples was markedly increased compared to that seen in control samples, but no changes were observed in either the total homogenate or cytoplasmic fractions (Fig. 2E, F and G). Immunoblot analysis with CaN showed similar intensity of full-length CaN in all three compartments between AD and control (Fig. 2H). By contrast, we observed a consistent 2.2-fold increase in the level of a 45-kDa fragment of CaN, a post-translationally truncated form of CaN (CaNCA), which is constitutively active, in the nuclear fraction in AD samples compared with control samples (Fig. 2I). This proteolytic product removes the autoinhibitory C-terminal domain, and has been observed as a mechanism of CaN activation in stroke, trauma, and glaucoma (Morioka et al., 1999; Wu et al., 2004; Burkard et al., 2005; Huang et al., 2005). Taken together, the aberrant accumulation of nuclear NFATc4 and constitutively active form of CaN indicate aberrant activation of CaN / NFATc4 signaling in AD. These results confirm the observation of truncated CaN in AD by Liu et al (Liu et al., 2005), but appear to contrast with those of Celsi et al (Celsi et al., 2007) who observed diminished CaN immunoreactivity in neurons in AD, perhaps because the latter study did not distinguish full length from truncated forms.

Conditioned media of Tg culture and Aβ oligomers isolated by Size Exclusion Chromatograpy (SEC) - induces NFATc4 nuclear translocation in wild-type neurons, which is blocked by Aβ immunodepletion or CaN inhibition

Soluble plaque-associated bioactive molecules, possibly assemblies of Aβ, may be responsible for the "halo" effect of neuritic change and $[Ca^{2+}]i$ alterations near plaques (Kuchibhotla et al., 2008; Meyer-Luehmann et al., 2008; Koffie et al., 2009). To examine this possibility, we studied the effect of Tg neuronal culture conditioned medium on CaN activation and neurite properties of wild-type neurons. Wild-type cortical neurons were cultured in standard NB/B27-serum free medium and at 14 DIV, the medium was replaced with diluted 1:4 CM from wild-type or Tg cultures for 24 hrs. As shown in Fig. 3B and C, neurons treated with wtCM for 24 hrs exhibited a relatively low nucleus/cytoplasm ratio of NFATc4, which was similar to neurons in culture without CM replacement. In contrast, neurons treated with Tg CM for 24 hrs demonstrated a significant increase in the nucleus/cytoplasm ratio of NFATc4 compared to neurons maintained in wtCM. The increased ratio was considerably reduced in neurons overexpressing an adeno-associated virus encoding an epitope-tagged (flag) AKAP79

fragment (AAV-AKAP79), a potent CaN inhibitory peptide (Coghlan et al., 1995) (Fig. 3A). Immunodepletion of Aβ from the Tg CM with 3D6 prevented the increase in the nucleus/cytoplasm ratio of NFATc4 (Fig. 3B and C), suggesting that soluble Aβ species in the Tg CM mediated activation of CaN and NFATc4 nuclear translocation. To better characterize the specific role of Aβ oligomers in CaN-mediated NFATc4 activation, non-denaturing SEC was used to isolate the various Aβ species from Tg CM. Both ELISA and Western blot analysis showed that SEC fractions 17–20 of Tg CM, but not the same fractions of wtCM, were markedly enriched in either oligomeric forms of Aβ 40 and 42 (supplemental Fig. 2E, F and G). Application of SEC fractions 18–19 (oligomeric Aβ fraction) of Tg CM onto wild-type neurons for 24 hours caused a significant increase in translocation of NFATc4 to the nucleus, but no changes were observed in neurons treated with the same SEC fractions of wtCM. Immunodepletion of Aβ from the fractions 18–19 of Tg CM with 3D6 prevented the increase in the nucleus/cytoplasm ratio of NFATc4 (Fig. 3D). Wild type neurons treated with fractions 6–7 (sAPP fraction, supplemental Fig. 2E, F and G) either from Tg CM or wtCM showed no significant difference in the nucleus/cytoplasm ratio of NFATc4. These results suggest that either Aβ containing CM from Tg culture or SEC-isolated Aβ oligomers is capable of inducing CaN-mediated NFATc4 activation.

Aβ containing conditioned medium causes morphological abnormalities in wild-type neurons identical to those observed in Tg neurons in culture

To test whether the abnormal morphology observed in Tg cultures is caused by Aβ, we examined wild-type cultured cortical neurons growing in either Tg or wild-type CM starting 24 hrs after plating and maintained in CM until neuron maturity (24 DIV). As shown in Fig. 4A, wild-type cultures maintained in Tg CM exhibited a significantly higher number of neurons with focal neuritic dystrophies compared to cultures maintained in wtCM. Cultures maintained in Tg CM that was pre-immunodepleted by 3D6, but not boiled 3D6, had a lower number of neurons with dystrophies similar to that seen in cultures growing in wtCM. Sholl analysis indicated that neurons growing in Aβ containing Tg CM also had dendritic simplification, but this is not the case in cultures maintained in Tg CM that was immunodepleted by 3D6 (Fig. 4B and C). A striking effect of Tg CM on dendritic spine density was also noted. The density of dendritic spines in the neurons growing in Tg CM was greatly decreased (Fig. 4D). There was no significant reduction of spine density between neurons growing in wtCM and Tg CM that was immunodepleted by 3D6, whereas spine density from neurons growing in Tg CM that was treated with inactive, boiled 3D6 was also significantly reduced. In addition, Tg neurons grown in media immunodepleted with 3D6 at 3 DIV no longer developed dystrophic morphology during maturation. We detected no statistically significant difference in the number of neurons with dystrophies (Fig. 4E), dendritic complexicity (Fig. 4F and G), or the mean spine density (Fig. 4H), between wild type and Tg neurons treated with media that had been immunodepleted by 3D6. These results suggest that Aβ immunodepletion blocks neurodegenerative morphologies that occur in neurons exposed to Aβ-containing CM, or that overexpress APP.

Inhibition of either CaN activity or CaN-mediated NFAT activation abolishes Tg CM or APP overexpression induced morphological abnormalities

Both CaN-mediated NFATc4 activation and abnormal morphologies were detected in Tg neurons and in wild-type neurons growing in Tg CM. We reasoned that Aβ might cause the morphological changes via CaN activation, or CaN activation and morphologic changes might each be unrelated effects of Aβ treatment. To address whether CaN is involved in the development of Aβ-related abnormal morphologies, wild-type neurons growing in Tg CM at 3DIV were transduced with an AAV encoding a CaN inhibitory peptide AKAP79. At 14 DIV essentially 100% of neurons expressed AKAP79 by measuring the co-localization of flag-tag positive neurons and MAP2 stained neurons (supplemental Fig. 3A). Tg neurons

overexpressing AKAP79, but not a control vector, AAV-β-galactosidase, contained significantly fewer neurons with beaded processes at 21 DIV (Fig. 5A). AKAP79 overexpression abolished Tg CM induced dendritic simplification as assessed by Sholl analysis (Fig. 5B and C) and reduction in dendritic spine density (Fig. 5D). In addition, Tg neurons overexpressing AKAP79 inhibitory peptide at an early time point (3 DIV) no longer developed dystrophic morphology during maturation. We detected no statistically significant difference in the number of neurons with dystrophies (Fig. 5E), dendritic complexity (Fig. 5F and G), and the mean spine density (Fig. 5H), between wild-type and Tg neurons overexpressing AKAP79 inhibitory peptide. FK506, a potent inhibitor of CaN with an independent mechanism of action, also blocked TgCM induced dendritic spine loss (supplemental Fig. 3B). These results suggest that CaN inhibition blocks neurodegenerative morphologies that occur in neurons exposed to Aβ-containing CM, or that overexpress APP.

CaN-mediated activation of NFAT has been demonstrated to play an important role in axonal outgrowth and activity-dependent dendritic structural changes during development (Graef et al., 2003; Groth and Mermelstein, 2003; Schwartz et al., 2009). Our present study indicates that nuclear accumulation of NFATc4 occurs in neurons from Tg cultures and in human AD postmortem brain, and that Aβ containing CM from Tg culture is capable of inducing CaN-mediated NFATc4 nuclear localization in wild type neurons. To clarify the signaling pathway activated by CaN that could involve CaN-dependent morphological neurodegeneration during Aβ neurotoxicity, we examined the effect of 11R-VIVIT (VIVIT), a cell-permeable peptide that blocks the docking sites for CaN-NFAT interaction and therefore specifically inhibits CaN-mediated NFAT activation without impacting other CaN substrates (Aramburu et al., 1999). Application of 2 µM VIVIT to wild type neurons growing in Tg CM abolished Tg CM induced NFAT nuclear accumulation (supplemental Fig. 3C and D), and blocked morphological deficits induced by Aβ, including reduced numbers of neurons with dendritic dystrophies (Fig. 6A), increased dendritic complexicity (Fig. 6B and C) and spine density (Fig. 6D). Similarly, Tg neurons treated with VIVIT showed dramatically improved morphology in comparison with Tg neurons treated with carrier (DMSO) (Fig. 6E, F, G and H). No significant changes in number of neurons with dendritic dystrophies, dendritic processes and spine density were detected in wild-type neurons treated with VIVIT or DMSO, suggesting that inhibition of CaN-NFAT interaction at the concentration that we are using does not have a strong effect on baseline maturation. Thus, inhibition of CaN-NFAT interaction and subsequent NFAT nuclear accumulation by VIVIT blocks Tg CM or APP overexpression induced morphological abnormalities in culture. These data indicate that upregulation of CaN activity by Aβ activates the NFAT cascade, resulting in a pathological triad of dendritic spine loss, dendritic simplification, and neuritic dystrophies.

Transduction of a CaNCA into wild-type cultured neurons induces abnormal morphology which is a phenocopy of the Aβ effect

To examine whether CaN activation is sufficient to cause these morphologic changes, even in the absence of overexpressed APP or exogenously applied Aβ, we investigated whether the expression of a CaNCA would favor morphological changes in wild-type cultured neurons. An AAV vector encoding a HA-tagged CaNCA (AAV-CaNCA) or wild-type CaN (AAV-CaNwt), or an AAV-vector control was expressed in cortical cultures. HA-tag immunostaining showed that nearly all MAP2 stained neurons expressed AAV-CaNwt or AAV-CaNCA, and neurons overexpressing CaNCA had significantly increased NFAT-luciferase activity, which was blocked by AKAP79 inhibitor peptide (supplemental Fig. 4A and B). As shown in Fig. 7A and B, neurons with swollen dendrites were barely detectable in CaNwt overexpressing cultures, but they were prominently detected in CaNCA overexpressing cultures. Approximately 15% of total GFP-positive neurons were observed to have typical local neuritic dystrophies in cultures overexpressing CaNCA (Fig. 7A and B), whereas, 6% of total GFP-

positive neurons developed dystrophies in CaNwt expressing cultures. The latter is similar to the number of dystrophic neurites found in cultures expressing β-galactosidase, an AAV-vector control. Dendritic complexicity (Fig. 7C and D) and mean spine density (Fig. 7E and F) were reduced in neurons overexpressing CaNCA, but not in CaNwt or vector overexpressing neurons. Inclusion of AKAP79 inhibitory peptide or VIVIT virtually eliminated CaNCA overexpression induced dendritic spine loss (supplemental Fig. 4C), suggesting that NFAT activation is critical for CaNCA-induced dendritic spine loss. These data indicate that ectopic expression of CaNCA is sufficient to cause neuritic dystrophies, dendritic simplication, and spine loss in neurons in culture.

CaNCA induces abnormal neuronal morphologies *in vivo*

To investigate the role of elevated CaN activity on neuronal morphology in the intact adult mouse brain, we next introduced high-titer AAV-CaNCA, AAV-CaNwt, or AAV-β-galactosidase, along with AAV-GFP, intracranially into the somatosensory cortex or hippocampus of C57Bl/6J mice by stereotaxic injection, as described in Materials and Methods. Three to four weeks after intracranial injection, GFP-filled neurites and corresponding spines were detectable in the live animals using multiphoton microscopy (Fig. 8C)(Spires et al., 2005). GFP labeled neurons were also observed in limited cortical and hippocampal areas in post mortem sections stained with a GFP antibody (Fig. 8A). We confirmed, with HA-tag staining, that almost all of the GFP positive cells were immunoreactive for CaNwt (or CaNCA), showing that GFP labeled neurons also expressed CaNwt or CaNCA (supplemental Fig. 5A). Compared with neurons expressing control vector or CaNwt, CaNCA expressing neurons showed high levels of NFATc4 nuclear distribution (supplemental Fig. 5A). The dendritic morphology of GFP-labeled neurites from cortical and hippocampal areas of wild-type mice injected with CaNCA displayed neurodegenerative alterations. Dystrophies were observed along the length of dendrites (Fig. 8B2) or axons (Fig. 8B4), whereas, dendrites or axons from these area of mice injected with CaNwt showed normal processes (Fig. 8B1, B3), similar to those seen in vector control injected mice. High power images from multiphoton observations of the live brain allowed analysis of dendritic spines, which showed that, compared to the control, spine density was significantly decreased in mice injected with CaNCA, whereas CaNwt injected mice showed mean spine density comparable to control vector injected mice (Fig. 8C and D).

Overexpression of a genetically encoded CaN inhibitor AKAP79 inhibitory peptide reduces Aβ associated neurodegenerative alterations *in vivo*

To directly determine the effect of CaN inhibition on the Aβ-related morphological abnormalities in the adult rodent brain *in vivo*, AAV-AKAP79 inhibitory peptide or a vector control was co-injected with AAV-GFP into somatosensory cortex in 6-month-old living APP/PS1 mice. With multi-photon imaging, we were able to quantitatively compare neuritic dystrophies (size of dystrophies defined as areas of swelling >2.5 µm in diameter), neurite curvature, as well as spine density near (< 50 µm) or far (> 50 µm) from amyloid deposits in living APP/PS1 mice. As shown in Fig. 9, the mean size of dystrophies near plaques from control vector injected brain was significantly larger than that found in brain injected with AKAP79 (Fig. 9A2, A3 and B). Compared to the vector control, spine density was significantly increased near plaques in mice injected with AKAP79 inhibitory peptide (Fig. 9C).

Another well-characterized morphological alteration in both APP over-expressing mouse brain and human AD is the development of tortuous, nonlinear trajectories for neurites, especially near plaques (Knowles et al., 1999; Le et al., 2001). This tortuosity is measured by "neuronal curvature", a marker of how straight a neurite segment is (Knowles et al., 1999). Compared to the elevated neuritic curvature seen at baseline in the APP/PS1 mice, we observed a significant improvement in neurite curvature in AKAP79 inhibitory peptide injected mice (Fig. 9D). Both

GFP and AKAP79 inhibitory peptide were co-expressed in the vast majority of neurons (supplemental Fig. 5B). Examination of Aβ deposits revealed no changes in the Aβ deposits themselves associated with AAV injection.

To exclude the possibility that *in vivo* imaging of GFP in neuritic dystrophies might not be representative, we examined SMI312 immunoreactivity, which recognizes a neurofilament protein that labels all axons, in postmortem sections. In the postmortem samples in control areas not expressing AKAP79 inhibitory peptide, axons in close proximity to Aβ deposits had abnormal large dystrophies as expected (Fig. 9E1). By contrast, substantially fewer axons in the AKAP79 inhibitory peptide injected areas in close proximity to Aβ deposits showed dystrophies (Fig. 9E2 and 9F). Consistent with the live imaging data, the mean size of dystrophies from control vector injected brain was significantly larger than those found in areas injected with AKAP79 inhibitory peptide (data not shown). Together, these results show that CaN inhibition blocks the neurodegenerative changes that are well-established to occur in the immediate vicinity of Aβ plaques *in vivo*, without affecting the Aβ deposits.

Discussion

Although it has been clear for a century that amyloid plaques are surrounded by neuritic abnormalities, and the amyloid hypothesis of AD suggests that Aβ peptide induces downstream neurodegenerative changes leading ultimately to collapse of neural networks and clinical dementia (Hardy and Allsop, 1991; Hardy and Selkoe, 2002), the molecules and mechanisms underlying the translation of Aβ neurotoxicity into morphological disruption remain undefined. Here we present data that support the idea that activation of CaN and subsequent NFAT-mediated downstream cascades are key molecular mechanisms linking Aβ to damage of the structural underpinnings of neural networks. This molecular model of neuronal degeneration is initiated by Aβ inducing calcium influx and CaN activation, which causes NFAT nuclear accumulation, leading to a pathological triad of dendritic spine loss, dendritic simplification, and neuritic dystrophies. Importantly, we show reversal of morphological neurodegenerative phenotypes *in vitro* and *in vivo* with a neuroprotective strategy of CaN inhibition, providing an important proof in principle of a non-Aβ directed therapeutic intervention that improves neuronal structure in an AD model.

Memory loss in AD patients is correlated strongly with synaptic dysfunction (DeKosky and Scheff, 1990; Terry et al., 1991; Sze et al., 1997). CaN is a protein phosphatase that plays a fundamental role in memory formation through mechanisms controlling synaptic function (Malleret et al., 2001; Winder and Sweatt, 2001; Mansuy, 2003). Mice with inducible, hippocampal-restricted overexpression of CaNCA exhibit pronounced spatial learning and memory deficits in the Morris water maze task (Mansuy, 2003). The defect of learning behaviors is reversible in transgenic mice expressing a CaN inhibitory domain or application of antisense oligonucleotides (Malleret et al., 2001; Mansuy, 2003). These results suggest that synaptic dysfunction and memory retention deficits that occur in AD patients and animal AD models may result, at least in part, from altered CaN activity. Indeed, CaN inhibition with FK-506 has been reported to improve memory function in APP transgenic mice (Dineley et al., 2007; Taglialatela et al., 2009).

In the present study, we have shown that neurons from Tg cultures exhibit increased NFATc4 nuclear translocation (Fig. 2A and B), which is known to be regulated by CaN activation. The NFATc4 - aberrant nuclear localization can also be induced by Tg CM, which contains high levels of naturally secreted Aβ, and this can be blocked by immunodepletion of the Tg CM with an Aβ-specific antibody, by the potent CaN inhibitory peptide AKAP79, or by treatment with VIVIT which blocks NFAT activation (Fig. 3B and C, supplemental Fig. 3C and D). Importantly, the NFATc4 - aberrant nuclear localization and a constitutively active form of

CaN were also found in AD postmortem brain, indicating that CaN activation and the resulting downstream NFAT transcriptional cascade also occurs in AD. Moreover, in cultures, CaN inhibition or blockade of NFAT activation using VIVIT provided significant neuroprotection from Tg CM or APP overexpression induced morphological deficits (Fig. 5 and Fig. 6).

CaN activation has profound effects on neuronal morphology. We show, both in cultures and in wild-type adult mouse brain *in vivo*, that manipulation of CaN activity by ectopic expression of CaNCA is sufficient to cause segmental spine loss, dendritic simplification and focal swelling similar to Aβ-induced morphological aberrations (Fig. 7 and Fig. 8). In mouse models of AD, CaN inhibition potently reduces the Aβ-related morphological neurodegenerative changes that occur near plaques (Fig. 9). These data suggest a pivotal novel role of CaN activation and CaN-mediated NFAT signaling pathway in Aβ-related morphological neurodegeneration, providing a mechanistic link between calcium overload, activation of CaN, and Aβ-induced neuronal morphological destruction of neural systems.

There are three major implications of these studies. First, our results confirm that Aβ induces CaN activation *in vitro* and in AD (Liu et al., 2005; Snyder et al., 2005; Hsieh et al., 2006; Agostinho et al., 2008; Reese et al., 2008; Abdul et al., 2009); we now show that CaN activation in neurons causes the pathological triad of dendritic spine loss, dendritic simplification, and dystrophies. Although it seems likely that activation of CaN has multiple effects, including functions at the dendritic spines itself (Hsieh et al., 2006), and it remains possible that VIVIT disrupts CaN functions other than NFAT dephosphorylarion (Oliveria et al., 2007), our data are consistent with the possibility that NFAT mediated cascades play a prominent role in the neurodegenerative process. These results clearly implicate a soluble form of Aβ, likely oligomeric, as the responsible bioactive molecule that is present in the vicinity of plaques that mediates the neuronal alterations that occur within a halo near plaques (Koffie et al., 2009). Importantly, these results allow the development of a simple *in vitro* model of Aβ-induced neurodegeneration (TgCM treatment of wild-type neurons for 24 hrs) that has predictive value for plaque-induced neurodegeneration in 8–12 month old transgenic animals.

Secondly, activated CaN produces a phenocopy of these Aβ effects. Importantly, either immunodepletion of Aβ, inhibition of CaN, or blockade of NFAT alone can inhibit these changes and lead to recovery of neuronal structure. Previous studies have shown some recovery of neuronal lesions after treatment with antibodies directed against Aβ (Lombardo et al., 2003; Brendza et al., 2005; Spires-Jones et al., 2008). Since our current data show that CaN activation is downstream of soluble Aβ neurotoxic effects, it seems likely that a strategy aimed at preventing or restoring CaN-mediated neural system damage, combined with approaches that reduce Aβ generation or promotes its clearance, may be more effective than either strategy alone. The higher enrichment of activated CaN and NFATc4 in the nuclear fraction of cortex from AD patients (Fig. 2E–I) reinforces the importance and disease-relevance of these observations. Thus, CaN inhibition or blockade of NFAT or its targets may be an important avenue for consideration in AD therapeutics.

Thirdly, our results suggest for the first time that CaN and NFAT play a major role in sculpting neural systems in the mature brain, implying that the adult brain is not "hard wired". A prominent role for CaN has been long established in learning and memory (Malleret et al., 2001; Winder and Sweatt, 2001; Zeng et al., 2001; Mansuy, 2003) and CaN activation is important in phenomena such as long term depression. A recent study suggests that CaN / NFAT signaling is responsible for dendritic simplification during developmental pruning of the Xenopus neural system (Schwartz et al., 2009). However, a major role for CaN-NFAT mediated transcriptional events in dendrite remodeling in the adult brain or in disease conditions as observed here has not been previously reported. Since aberrant CaN activation has been implicated in CNS trauma, ischemia, Kainate injury, and glaucoma (Morioka et al.,

1999; Springer et al., 2000; Wu et al., 2004; Huang et al., 2005; Uchino et al., 2008), each of which leads to neural system degeneration, we postulate that the type of structural remodeling and morphological degenerative changes observed in multiple conditions might be a consequence of CaN activation. Intriguingly, it appears as if the major effects of CaN in AD may be mediated by NFAT, implying a potential unexplored role for transcriptional cascades in these conditions. Thus, a molecular mechanism of neurodegeneration in AD may be Aβ-induced aberrant activation of a potent NFAT-mediated developmental program of neural system remodeling, suggesting possible therapeutic avenues for rescue.

Supplementary Material

Refer to Web version on PubMed Central for supplementary material.

Acknowledgments

References

Abdul HM, Sama MA, Furman JL, Mathis DM, Beckett TL, Weidner AM, Patel ES, Baig I, Murphy MP, LeVine H 3rd, Kraner SD, Norris CM. Cognitive decline in Alzheimer's disease is associated with selective changes in calcineurin/NFAT signaling. J Neurosci 2009;29:12957–12969. [PubMed: 19828810]

Agostinho P, Lopes JP, Velez Z, Oliveira CR. Overactivation of calcineurin induced by amyloid-beta and prion proteins. Neurochem Int 2008;52:1226–1233. [PubMed: 18295934]

Aramburu J, Yaffe MB, Lopez-Rodriguez C, Cantley LC, Hogan PG, Rao A. Affinity-driven peptide selection of an NFAT inhibitor more selective than cyclosporin A. Science 1999;285:2129–2133. [PubMed: 10497131]

Bacskai BJ, Hickey GA, Skoch J, Kajdasz ST, Wang Y, Huang GF, Mathis CA, Klunk WE, Hyman BT. Four-dimensional multiphoton imaging of brain entry, amyloid binding, and clearance of an amyloid-beta ligand in transgenic mice. Proc Natl Acad Sci U S A 2003;100:12462–12467. [PubMed: 14517353]

Berridge MJ, Lipp P, Bootman MD. The versatility and universality of calcium signalling. Nat Rev Mol Cell Biol 2000;1:11–21. [PubMed: 11413485]

Bezprozvanny I, Mattson MP. Neuronal calcium mishandling and the pathogenesis of Alzheimer's disease. Trends Neurosci 2008;31:454–463. [PubMed: 18675468]

Brendza RP, Bacskai BJ, Cirrito JR, Simmons KA, Skoch JM, Klunk WE, Mathis CA, Bales KR, Paul SM, Hyman BT, Holtzman DM. Anti-Abeta antibody treatment promotes the rapid recovery of amyloid-associated neuritic dystrophy in PDAPP transgenic mice. J Clin Invest 2005;115:428–433. [PubMed: 15668737]

Burkard N, Becher J, Heindl C, Neyses L, Schuh K, Ritter O. Targeted proteolysis sustains calcineurin activation. Circulation 2005;111:1045–1053. [PubMed: 15723976]

Busche MA, Eichhoff G, Adelsberger H, Abramowski D, Wiederhold KH, Haass C, Staufenbiel M, Konnerth A, Garaschuk O. Clusters of hyperactive neurons near amyloid plaques in a mouse model of Alzheimer's disease. Science 2008;321:1686–1689. [PubMed: 18802001]

Celsi F, Svedberg M, Unger C, Cotman CW, Carri MT, Ottersen OP, Nordberg A, Torp R. Beta-amyloid causes downregulation of calcineurin in neurons through induction of oxidative stress. Neurobiol Dis 2007;26:342–352. [PubMed: 17344052]

Coghlan VM, Perrino BA, Howard M, Langeberg LK, Hicks JB, Gallatin WM, Scott JD. Association of protein kinase A and protein phosphatase 2B with a common anchoring protein. Science 1995;267:108–111. [PubMed: 7528941]

DeKosky ST, Scheff SW. Synapse loss in frontal cortex biopsies in Alzheimer's disease: correlation with cognitive severity. Ann Neurol 1990;27:457–464. [PubMed: 2360787]

Dineley KT, Hogan D, Zhang WR, Taglialatela G. Acute inhibition of calcineurin restores associative learning and memory in Tg2576 APP transgenic mice. Neurobiol Learn Mem 2007;88:217–224. [PubMed: 17521929]

Geula C, Wu CK, Saroff D, Lorenzo A, Yuan M, Yankner BA. Aging renders the brain vulnerable to amyloid beta-protein neurotoxicity. Nat Med 1998;4:827–831. [PubMed: 9662375]

Graef IA, Wang F, Charron F, Chen L, Neilson J, Tessier-Lavigne M, Crabtree GR. Neurotrophins and netrins require calcineurin/NFAT signaling to stimulate outgrowth of embryonic axons. Cell 2003;113:657–670. [PubMed: 12787506]

Groth RD, Mermelstein PG. Brain-derived neurotrophic factor activation of NFAT (nuclear factor of activated T-cells)-dependent transcription: a role for the transcription factor NFATc4 in neurotrophin-mediated gene expression. J Neurosci 2003;23:8125–8134. [PubMed: 12954875]

Halpain S, Hipolito A, Saffer L. Regulation of F-actin stability in dendritic spines by glutamate receptors and calcineurin. J Neurosci 1998;18:9835–9844. [PubMed: 9822742]

Hardy J, Allsop D. Amyloid deposition as the central event in the aetiology of Alzheimer's disease. Trends Pharmacol Sci 1991;12:383–388. [PubMed: 1763432]

Hardy J, Selkoe DJ. The amyloid hypothesis of Alzheimer's disease: progress and problems on the road to therapeutics. Science 2002;297:353–356. [PubMed: 12130773]

Hsiao K, Chapman P, Nilsen S, Eckman C, Harigaya Y, Younkin S, Yang F, Cole G. Correlative memory deficits, Abeta elevation, and amyloid plaques in transgenic mice. Science 1996;274:99–102. [PubMed: 8810256]

Hsieh H, Boehm J, Sato C, Iwatsubo T, Tomita T, Sisodia S, Malinow R. AMPAR removal underlies Abeta-induced synaptic depression and dendritic spine loss. Neuron 2006;52:831–843. [PubMed: 17145504]

Huang W, Fileta JB, Dobberfuhl A, Filippopoulos T, Guo Y, Kwon G, Grosskreutz CL. Calcineurin cleavage is triggered by elevated intraocular pressure, and calcineurin inhibition blocks retinal ganglion cell death in experimental glaucoma. Proc Natl Acad Sci U S A 2005;102:12242–12247. [PubMed: 16103353]

Johnson-Wood K, Lee M, Motter R, Hu K, Gordon G, Barbour R, Khan K, Gordon M, Tan H, Games D, Lieberburg I, Schenk D, Seubert P, McConlogue L. Amyloid precursor protein processing and A beta42 deposition in a transgenic mouse model of Alzheimer disease. Proceedings of the National Academy of Sciences of the United States of America 1997;94:1550–1555. [PubMed: 9037091]

Klee CB, Crouch TH, Krinks MH. Calcineurin: a calcium- and calmodulin-binding protein of the nervous system. Proc Natl Acad Sci U S A 1979;76:6270–6273. [PubMed: 293720]

Klunk WE, Bacskai BJ, Mathis CA, Kajdasz ST, McLellan ME, Frosch MP, Debnath ML, Holt DP, Wang Y, Hyman BT. Imaging Abeta plaques in living transgenic mice with multiphoton microscopy and methoxy-X04, a systemically administered Congo red derivative. J Neuropathol Exp Neurol 2002;61:797–805. [PubMed: 12230326]

Knowles RB, Wyart C, Buldyrev SV, Cruz L, Urbanc B, Hasselmo ME, Stanley HE, Hyman BT. Plaque-induced neurite abnormalities: implications for disruption of neural networks in Alzheimer's disease. Proc Natl Acad Sci U S A 1999;96:5274–5279. [PubMed: 10220456]

Koffie RM, Meyer-Luehmann M, Hashimoto T, Adams KW, Mielke ML, Garcia-Alloza M, Micheva KD, Smith SJ, Kim ML, Lee VM, Hyman BT, Spires-Jones TL. Oligomeric amyloid beta associates with postsynaptic densities and correlates with excitatory synapse loss near senile plaques. Proc Natl Acad Sci U S A 2009;106:4012–4017. [PubMed: 19228947]

Kuchibhotla KV, Goldman ST, Lattarulo CR, Wu HY, Hyman BT, Bacskai BJ. Abeta plaques lead to aberrant regulation of calcium homeostasis in vivo resulting in structural and functional disruption of neuronal networks. Neuron 2008;59:214–225. [PubMed: 18667150]

Le R, Cruz L, Urbanc B, Knowles RB, Hsiao-Ashe K, Duff K, Irizarry MC, Stanley HE, Hyman BT. Plaque-induced abnormalities in neurite geometry in transgenic models of Alzheimer disease: implications for neural system disruption. J Neuropathol Exp Neurol 2001;60:753–758. [PubMed: 11487049]

Liu F, Grundke-Iqbal I, Iqbal K, Oda Y, Tomizawa K, Gong CX. Truncation and activation of calcineurin A by calpain I in Alzheimer disease brain. J Biol Chem 2005;280:37755–37762. [PubMed: 16150694]

Lombardo JA, Stern EA, McLellan ME, Kajdasz ST, Hickey GA, Bacskai BJ, Hyman BT. Amyloid-beta antibody treatment leads to rapid normalization of plaque-induced neuritic alterations. J Neurosci 2003;23:10879–10883. [PubMed: 14645482]

Lorenzo A, Yankner BA. Beta-amyloid neurotoxicity requires fibril formation and is inhibited by congo red. Proc Natl Acad Sci U S A 1994;91:12243–12247. [PubMed: 7991613]

Malleret G, Haditsch U, Genoux D, Jones MW, Bliss TV, Vanhoose AM, Weitlauf C, Kandel ER, Winder DG, Mansuy IM. Inducible and reversible enhancement of learning, memory, and long-term potentiation by genetic inhibition of calcineurin. Cell 2001;104:675–686. [PubMed: 11257222]

Mansuy IM. Calcineurin in memory and bidirectional plasticity. Biochem Biophys Res Commun 2003;311:1195–1208. [PubMed: 14623305]

Mattson MP. Pathways towards and away from Alzheimer's disease. Nature 2004;430:631–639. [PubMed: 15295589]

Meyer-Luehmann M, Spires-Jones TL, Prada C, Garcia-Alloza M, de Calignon A, Rozkalne A, Koenigsknecht-Talboo J, Holtzman DM, Bacskai BJ, Hyman BT. Rapid appearance and local toxicity of amyloid-beta plaques in a mouse model of Alzheimer's disease. Nature 2008;451:720–724. [PubMed: 18256671]

Morioka M, Hamada J, Ushio Y, Miyamoto E. Potential role of calcineurin for brain ischemia and traumatic injury. Prog Neurobiol 1999;58:1–30. [PubMed: 10321795]

Mulkey RM, Endo S, Shenolikar S, Malenka RC. Involvement of a calcineurin/inhibitor-1 phosphatase cascade in hippocampal long-term depression. Nature 1994;369:486–488. [PubMed: 7515479]

Oliveria SF, Dell'Acqua ML, Sather WA. AKAP79/150 anchoring of calcineurin controls neuronal L-type Ca2+ channel activity and nuclear signaling. Neuron 2007;55:261–275. [PubMed: 17640527]

Palotas A, Kalman J, Palotas M, Juhasz A, Janka Z, Penke B. Fibroblasts and lymphocytes from Alzheimer patients are resistant to beta-amyloid-induced increase in the intracellular calcium concentration. Prog Neuropsychopharmacol Biol Psychiatry 2002;26:971–974. [PubMed: 12369273]

Pike CJ, Burdick D, Walencewicz AJ, Glabe CG, Cotman CW. Neurodegeneration induced by beta-amyloid peptides in vitro: the role of peptide assembly state. J Neurosci 1993;13:1676–1687. [PubMed: 8463843]

Reese LC, Zhang W, Dineley KT, Kayed R, Taglialatela G. Selective Induction of Calcineurin Activity and Signaling by Oligomeric Amyloid Beta. Aging Cell. 2008

Schwartz N, Schohl A, Ruthazer ES. Neural activity regulates synaptic properties and dendritic structure in vivo through calcineurin/NFAT signaling. Neuron 2009;62:655–669. [PubMed: 19524525]

Shankar GM, Bloodgood BL, Townsend M, Walsh DM, Selkoe DJ, Sabatini BL. Natural oligomers of the Alzheimer amyloid-beta protein induce reversible synapse loss by modulating an NMDA-type glutamate receptor-dependent signaling pathway. J Neurosci 2007;27:2866–2875. [PubMed: 17360908]

Shankar GM, Li S, Mehta TH, Garcia-Munoz A, Shepardson NE, Smith I, Brett FM, Farrell MA, Rowan MJ, Lemere CA, Regan CM, Walsh DM, Sabatini BL, Selkoe DJ. Amyloid-beta protein dimers isolated directly from Alzheimer's brains impair synaptic plasticity and memory. Nat Med 2008;14:837–842. [PubMed: 18568035]

Smith IF, Green KN, LaFerla FM. Calcium dysregulation in Alzheimer's disease: recent advances gained from genetically modified animals. Cell Calcium 2005;38:427–437. [PubMed: 16125228]

Snyder EM, Nong Y, Almeida CG, Paul S, Moran T, Choi EY, Nairn AC, Salter MW, Lombroso PJ, Gouras GK, Greengard P. Regulation of NMDA receptor trafficking by amyloid-beta. Nat Neurosci 2005;8:1051–1058. [PubMed: 16025111]

Spires-Jones TL, de Calignon A, Matsui T, Zehr C, Pitstick R, Wu HY, Osetek JD, Jones PB, Bacskai BJ, Feany MB, Carlson GA, Ashe KH, Lewis J, Hyman BT. In vivo imaging reveals dissociation between caspase activation and acute neuronal death in tangle-bearing neurons. J Neurosci 2008;28:862–867. [PubMed: 18216194]

Spires TL, Meyer-Luehmann M, Stern EA, McLean PJ, Skoch J, Nguyen PT, Bacskai BJ, Hyman BT. Dendritic spine abnormalities in amyloid precursor protein transgenic mice demonstrated by gene transfer and intravital multiphoton microscopy. J Neurosci 2005;25:7278–7287. [PubMed: 16079410]

Springer JE, Azbill RD, Nottingham SA, Kennedy SE. Calcineurin-mediated BAD dephosphorylation activates the caspase-3 apoptotic cascade in traumatic spinal cord injury. J Neurosci 2000;20:7246–7251. [PubMed: 11007881]

Stutzmann GE. Calcium dysregulation, IP3 signaling, and Alzheimer's disease. Neuroscientist 2005;11:110–115. [PubMed: 15746379]

Sze CI, Troncoso JC, Kawas C, Mouton P, Price DL, Martin LJ. Loss of the presynaptic vesicle protein synaptophysin in hippocampus correlates with cognitive decline in Alzheimer disease. J Neuropathol Exp Neurol 1997;56:933–944. [PubMed: 9258263]

Taglialatela G, Hogan D, Zhang WR, Dineley KT. Intermediate-and long-term recognition memory deficits in Tg2576 mice are reversed with acute calcineurin inhibition. Behavioural Brain Research 2009;200:95–99. [PubMed: 19162087]

Terry RD, Masliah E, Salmon DP, Butters N, DeTeresa R, Hill R, Hansen LA, Katzman R. Physical basis of cognitive alterations in Alzheimer's disease: synapse loss is the major correlate of cognitive impairment. Ann Neurol 1991;30:572–580. [PubMed: 1789684]

Townsend M, Shankar GM, Mehta T, Walsh DM, Selkoe DJ. Effects of secreted oligomers of amyloid beta-protein on hippocampal synaptic plasticity: a potent role for trimers. J Physiol 2006;572:477–492. [PubMed: 16469784]

Uchino H, Kuroda Y, Morota S, Hirabayashi G, Ishii N, Shibasaki F, Ikeda Y, Hansson MJ, Elmer E. Probing the molecular mechanisms of neuronal degeneration: importance of mitochondrial dysfunction and calcineurin activation. J Anesth 2008;22:253–262. [PubMed: 18685932]

Walsh DM, Selkoe DJ. Deciphering the molecular basis of memory failure in Alzheimer's disease. Neuron 2004;44:181–193. [PubMed: 15450169]

Wang JH, Kelly PT. The balance between postsynaptic Ca(2+)-dependent protein kinase and phosphatase activities controlling synaptic strength. Learn Mem 1996;3:170–181. [PubMed: 10456087]

Winder DG, Sweatt JD. Roles of serine/threonine phosphatases in hippocampal synaptic plasticity. Nat Rev Neurosci 2001;2:461–474. [PubMed: 11433371]

Wu HY, Tomizawa K, Oda Y, Wei FY, Lu YF, Matsushita M, Li ST, Moriwaki A, Matsui H. Critical role of calpain-mediated cleavage of calcineurin in excitotoxic neurodegeneration. J Biol Chem 2004;279:4929–4940. [PubMed: 14627704]

Yaari R, Corey-Bloom J. Alzheimer's disease. Semin Neurol 2007;27:32–41. [PubMed: 17226739]

Zeng H, Chattarji S, Barbarosie M, Rondi-Reig L, Philpot BD, Miyakawa T, Bear MF, Tonegawa S. Forebrain-specific calcineurin knockout selectively impairs bidirectional synaptic plasticity and working/episodic-like memory. Cell 2001;107:617–629. [PubMed: 11733061]
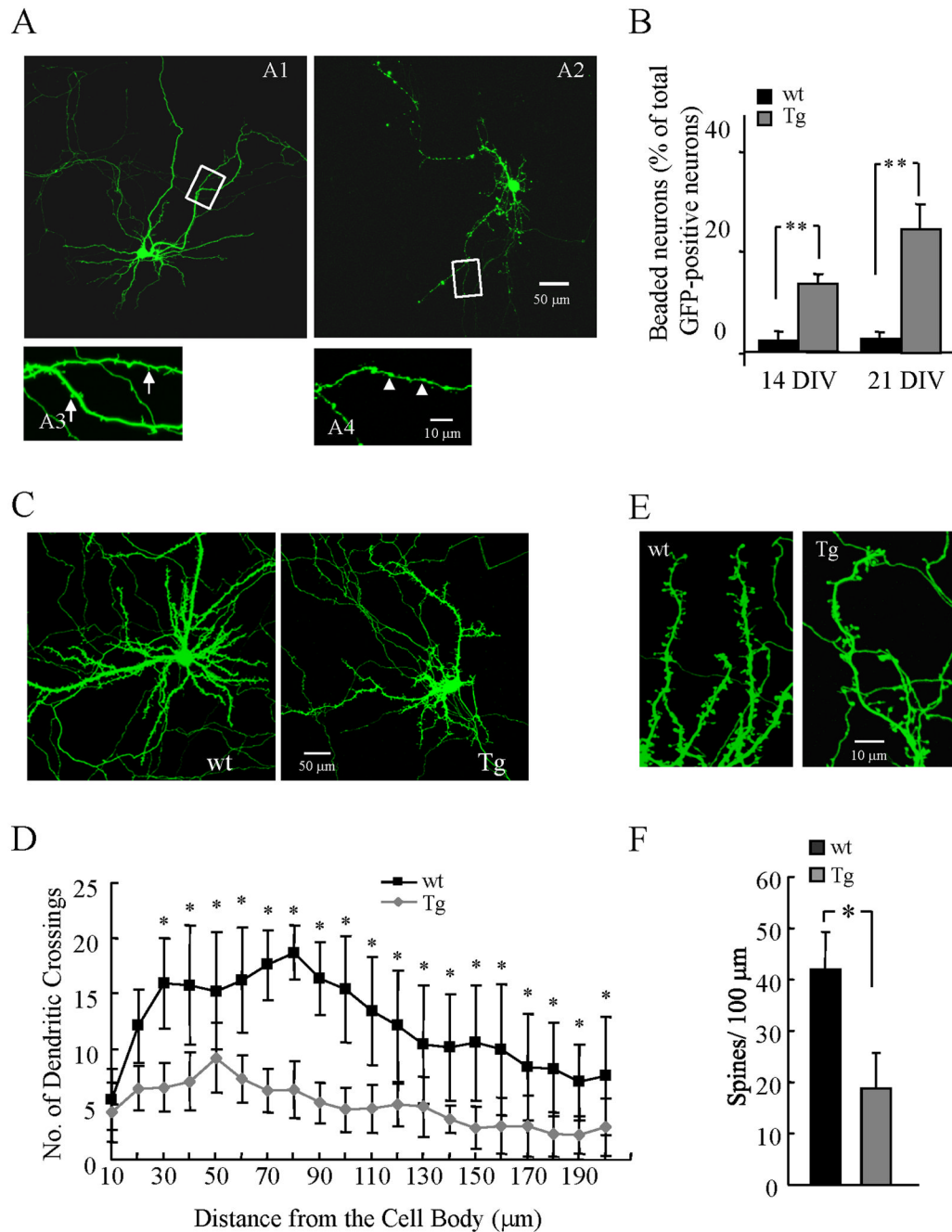
Figure 1.
Abnormal morphologies in neurons from Tg cultures. (**A**) Representative images of a wild-type GFP-labeled neuron at 14 DIV shows intricately branched dendritic arbors (*A*1 and *A*3), whereas Tg neurons exhibit simplified dendritic complexity and localized dendritic dystrophies (*A*2 and *A*4). (**B**) The percentage of neurons with dendritic dystrophies at 14 DIV and 21 DIV was increased in Tg neurons compared to wild-type. (14 DIV, wt cultures: $2.0 \pm 0.2\%$; Tg cultures: $14.0 \pm 2.0\%$, $p < 0.0001$; 21 DIV, wt cultures: $3.0 \pm 0.2\%$; Tg cultures: $24.0 \pm 5.0\%$, $p < 0.0001$ (wt vs Tg); $p = 0.0003$ (14 DIV vs 21 DIV). n = 50 cells from each condition. (**C**) Representative images of a wild-type or Tg GFP labeled mature neurons (21 DIV). (**D**) Sholl analysis of total number of branch point on basal dendrites of neuron from wild-type and Tg

cultures shows decreased complexity in Tg neurons starting at 30 µm from the cell body. n = 25 cells from each condition. (**E**) Representative GFP labeled dendritic segments studded with mature spines from wild-type and Tg neurons show a loss of spines on Tg dendrites that is confirmed in quantitative assay of spine densities determined in neurons without apparent dystrophies at 21 DIV in wild-type and Tg cultures (**F**). n = 4 culture/experiment and 400 spines from each condition. * $P < 0.05$; ** $P < 0.01$; Data represent mean ± SD.
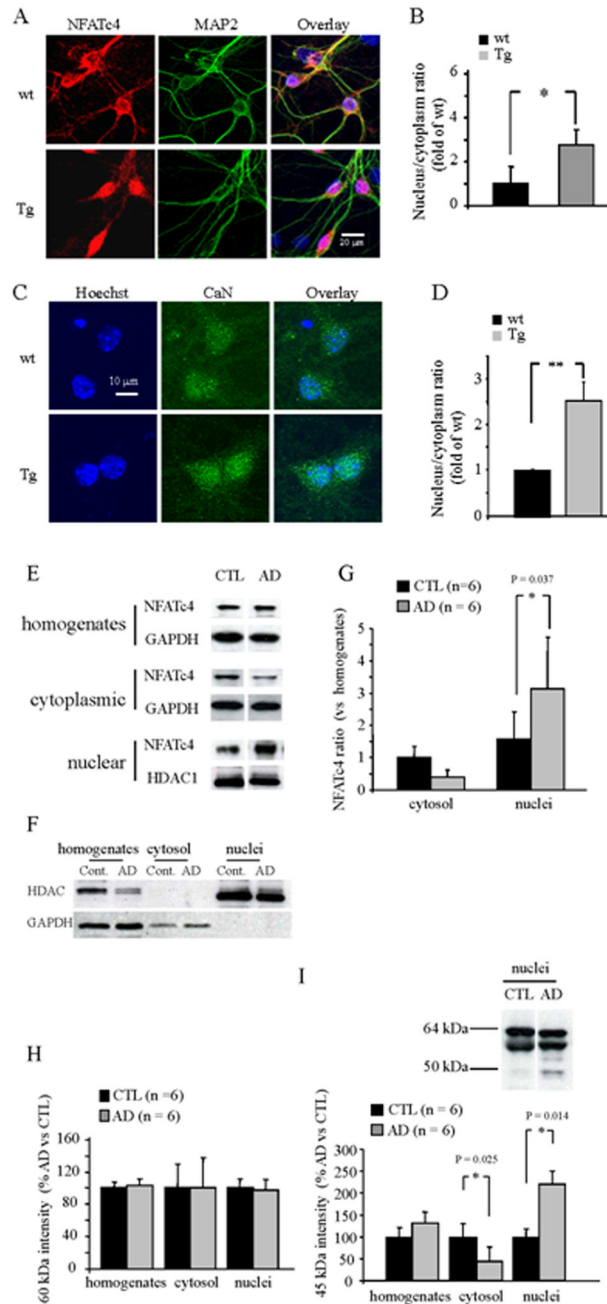
Figure 2.
Aβ induces NFATc4 and CaN aberrant nuclear localization in Tg neurons in culture and AD postmortem brains. (*A*) Immunostaining images of NFATc4 in Tg or wild-type neurons. Neurons from Tg or wild-type culture at 14 DIV are labeled with NFATc4 (red), MAP2 (green) and Hoechst nuclear counterstain (blue). Compared with wild-type neurons, Tg neurons show higher immunoreactivity of NFATc4 in the nuclei. (*B*) Quantification of NFATc4 nuclear immunoreactivity obtained from *A*. n = 40 cells from 3 different experiments, * $P < 0.05$; Data represent mean ± SD. (*C*) Immunostaining images of CaN in Tg or wild-type neurons. Neurons from Tg or wild-type culture at 14 DIV are labeled with CaN (green) and Hoechst nuclear counterstain (blue). Compared with wild-type neurons, Tg neurons show higher

immunoreactivity of CaN in the nuclei. (**D**) Quantification of CaN nuclear immunoreactivity obtained from *C*. n = 40. * *P* < 0.01; Data represent mean ± SD. (***E and F***) Subcellular fractions were prepared from brains of AD patients or controls and analyzed by immunoblotting for NFATc4 and cytoplasmic or nuclear control proteins GAPDH, HDAC1, respectively. (**G**) Semiquantification of NFATc4 immunoreactivity in *E*. NFATc4 was detected in all three compartments, but substantially enriched in nuclei in AD brains (n = 6 for each condition). * *P* < 0.05; Data represent mean ± SD. (***H*** and ***I***). Semiquantification of immunoreactivity from each subcellular fraction for both full-length CaN (60 kDa) (**H**) and CaNCA (45 kDa) (**I**). Insert in (*I*) shows representative blots of CaN in nuclear fraction. * *P* < 0.05; Data represent mean ± SEM.
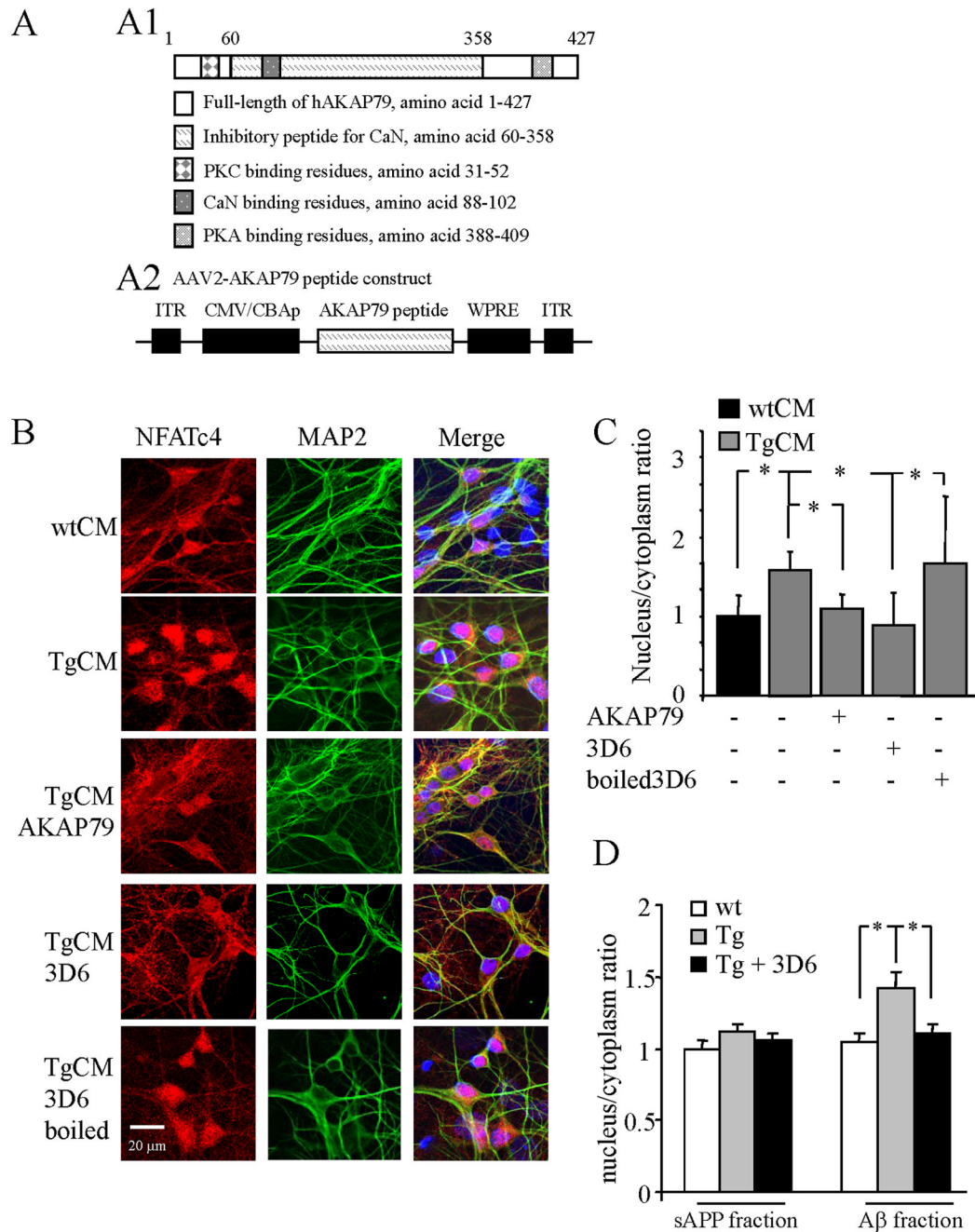
Figure 3.
Conditioned medium induces NFATc4 - aberrant nuclear translocation in wild-type cultured neurons. (*A*) Schematic representation of AKAP79 inhibitory peptide for CaN (*A1*) and AAV2 viral vectors (AAV-CMV/CBA-WPRE) with AKAP79 inhibitory peptide (*A2*). (*B*) Aβ depletion or CaN inhibition with AKAP79 inhibitory peptide prevents Tg CM induced NFATc4 activation as seen in cultures stained with NFATc4 (red), MAP2 (green) and Hoechst nuclear counterstain (blue) from each experimental condition. (*C*) Quantification of NFATc4 - aberrant nuclear translocation induced by TgCM in wild-type cultured neurons. The ratio of nucleus to cytosoplasm is shown. TgCM causes an increase in the nucleus/cytoplasm ratio of NFATc4 that is dependent upon the presence of Aβ (since anti-Aβ antibody 3D6 prevents the

effect). Inhibition of CaN activation by AKAP79 peptide also prevented the increase in the nucleus/cytoplasm ration of NFATc4 (n > 40 cells). Data represent mean ± SD. *, $P < 0.05$. **D**, Quantification of NFATc4 - aberrant nuclear translocation induced by different SEC-fractions in wild-type cultured neurons. Application of SEC fractions 6–7 (sAPP fraction) either from TgCM or wtCM caused no significant difference on the nucleus/cytoplasm ratio of NFATc4. However, application of SEC fractions 18–19 (Aβ fraction) of TgCM onto wild-type neurons for 24 hours caused significant increase in translocation of NFATc4 to the nucleus, but no changes were observed in neurons applied with the same SEC fractions of wtCM. Immunodepletion of Aβ from the fractions 18–19 of TgCM with 3D6 prevented the increase in the nucleus/cytoplasm ratio of NFATc4. (n > 35 cells). Data represent mean ± SD. *, $P < 0.05$.
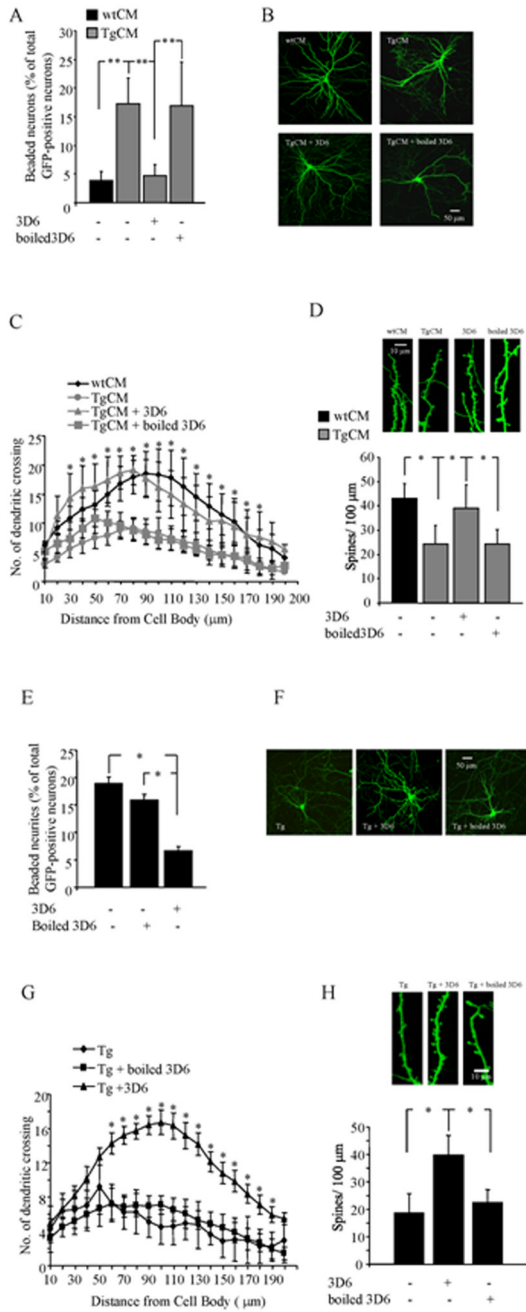
Figure 4.
Aberrant neuronal morphologies induced by TgCM or APP overexpressing are prevented by Aβ depletion. (*A*) Primary cultures were maintained in Tg CM for 21 DIV in different culture conditions, as indicated. The percentage of neurons with dendritic dystrophies at 21 DIV is increased in the presence of Tg CM, and this beading can be prevented by immunodepletion of Aβ. (*B* and *C*) Representative GFP labeled mature neurons (*B*) and Sholl analysis of branching on dendrites of neurons from indicated conditions shows that Tg CM reduced branching and that this is rescued by immunodepletion of Aβ with 3D6 (*C*). (*D*) Spine densities are determined in neurons without apparent dystrophies in each experimental condition, showing a decrease in spine density with Tg CM that could be rescued with 3D6 treatment.

(*E*, *F, G and H*) Aβ depletion prevents APP overexpression induced morphological abnormalities. In Tg cultures at 21 DIV, dendritic dystrophies (*E*), dendritic attenuation (*F and G*) and spine loss (*H*) are prevented by Aβ depletion with 3D6. 60 cells were analyzed per experimental condition in each experiment. *, $P < 0.05$; ** $P < 0.01$; * in *G*, indicates $p < 0.05$ (Tg with 3D6 vs Tg with boiled 3D6). Data represent mean ± SD.
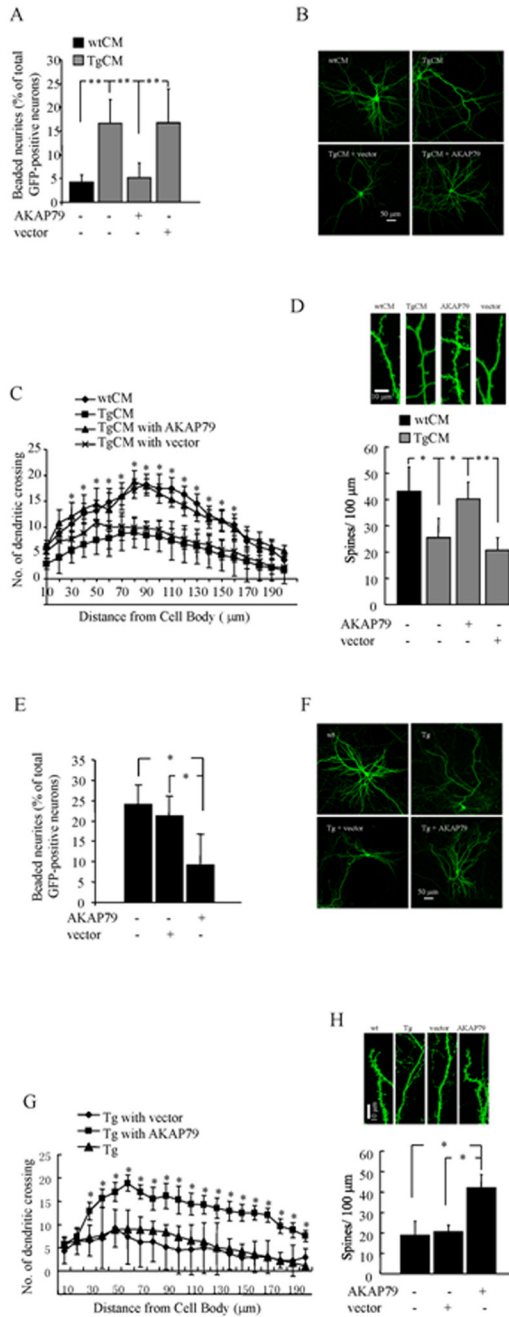
Figure 5.
CaN inhibition by AKAP79 inhibitory peptide prevents Tg CM induced morphological abnormalities. Dendritic dystrophies (*A*), dendritic attenuation (*B and C*) and spine loss (*D*) in wild-type cultured neurons growing in Tg CM are significantly prevented by CaN inhibitory peptide AKAP79. * in *C*, indicates statistical significance ($p < 0.05$; TgCM with AKAP79 vs TgCM with vector). Data are mean ± SD from three independent experiments in triplicate. (*E*, *F, G and H*) CaN inhibition by AKAP79 inhibitory peptide prevents APP overexpression induced morphological abnormalities. In Tg cultures at 21 DIV, dendritic dystrophies (*E*), dendritic attenuation (*F and G*) and spine loss (*H*) are prevented by CaN inhibitory peptide

AKAP79. * in *G*, indicates statistically significant (p < 0.05; Tg with AKAP79 vs Tg with vector). Data are mean ± SD from three independent experiments, each in triplicate.
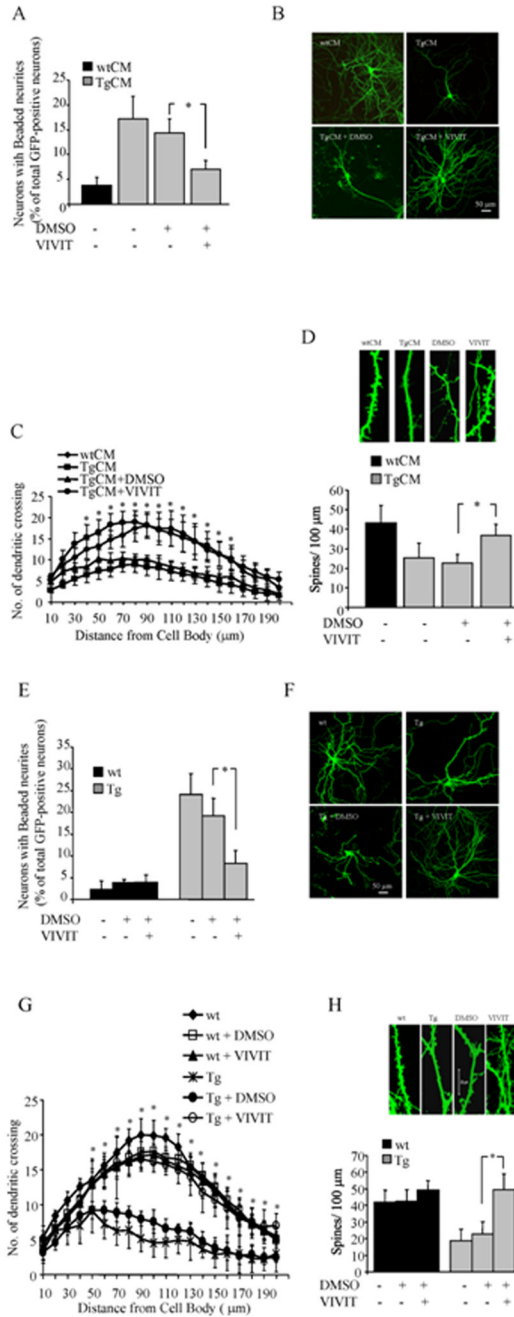
Figure 6.
Inhibition of CaN-NFAT interaction by VIVIT prevents Tg CM induced morphological abnormalities. Dendritic dystrophies (*A*), dendritic attenuation (*B and C*) and spine loss (*D*) in wild-type cultured neurons growing in Tg CM are significantly prevented by VIVIT (CALBIOCHEM, Cat# 480401). * in *C*, indicates statistically significant (p < 0.05; TgCM with VIVIT vs TgCM with DMSO). Data are mean ± SD from three independent experiments in triplicate. (*E*, *F, G and H*) Inhibition of CaN-NFAT interaction by VIVIT prevents APP overexpression induced morphological abnormalities. In Tg cultures at 21 DIV, dendritic dystrophies (*E*), dendritic attenuation (*F and G*) and spine loss (*H*) are prevented by VIVIT. *

in *G*, indicates statistically significant (p < 0.05; Tg with VIVIT vs Tg with DMSO). Data are mean ± SD from three independent experiments in triplicate.
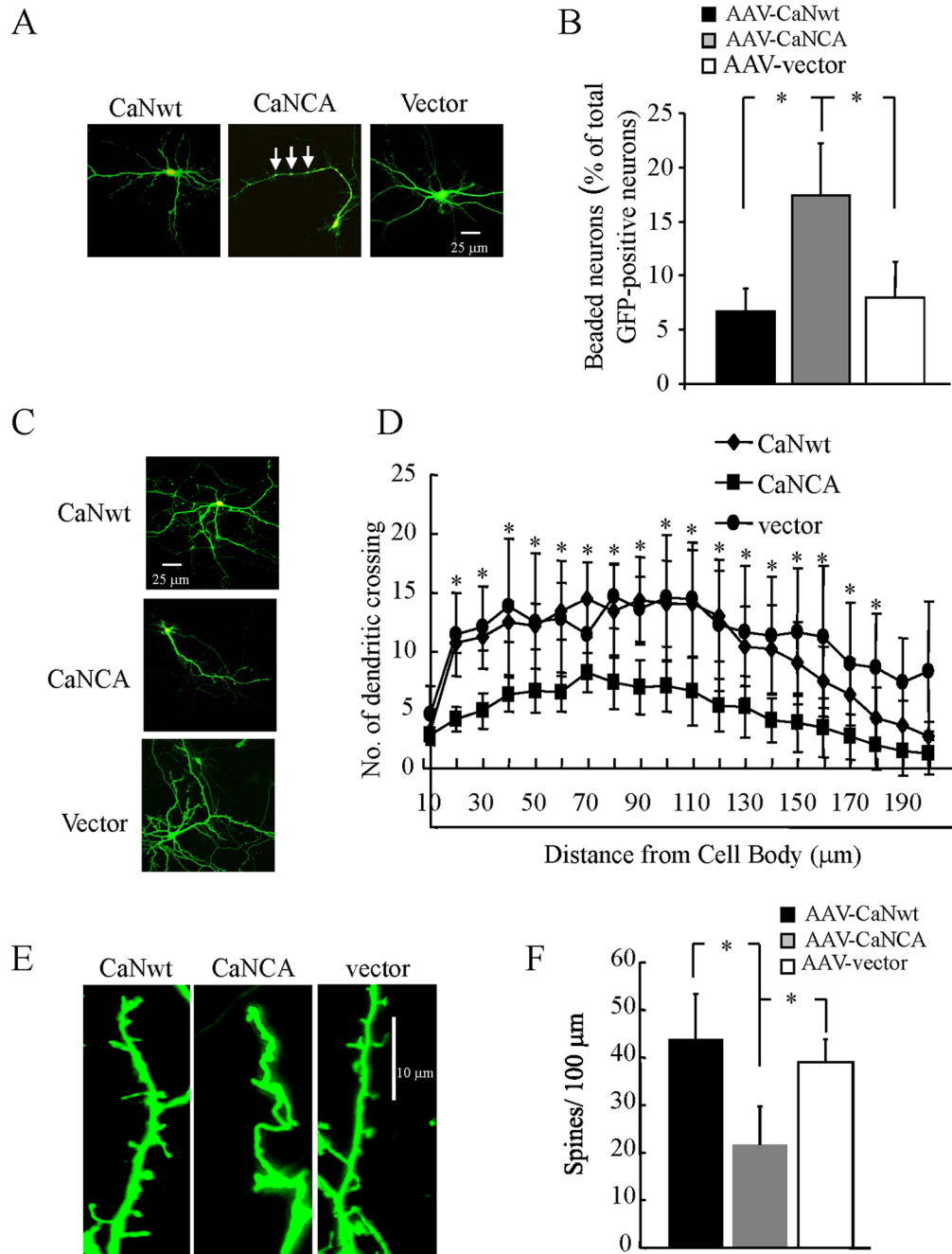
Figure 7.
Wild-type cultured neurons overexpressing a constitutively active CaN construct, CaNCA, develop abnormal morphology which is a phenocopy of the Aβ effect. Overexpression of CaNCA, but not CaNwt or vector control, into wild-type cultures induces dendritic dystrophies (*A* and *B*; arrows indicated local swelling of dendrites), simplification of dendritic arboration (*C* and *D*) and spine loss (*E* and *F*). Neurons expressing CaNCA displayed significantly more neurons with dendritic dystrophies, simplified dendritic complexity and spine loss than either CaNwt or vector expressing neurons. *, $p < 0.05$; * in *D*, indicates statistical significance ($p < 0.05$; CaNwt vs CaNCA). Data are mean ± SD from three independent experiments, each in triplicate.
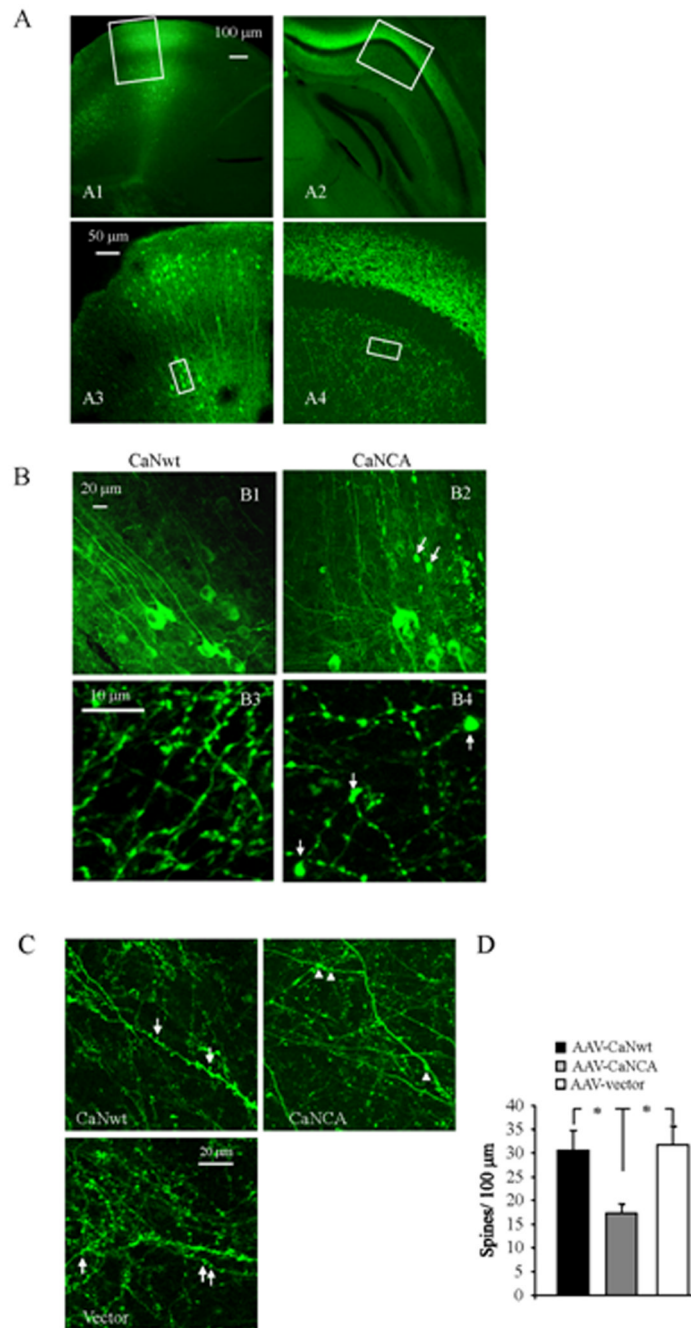
Figure 8.
Overexpression of CaNCA, but not CaNwt, in the intact mouse brain induces abnormal morphologies. (*A*) Representative images in different magnifications from cortex (*A*1 and *A*3) and hippocampal areas (*A*2 and *A*4) after CaNCA or CaNwt transduction showing GFP expression in fixed postmortem brain sections stained with GFP antibody. (*B*) Representative high power images of neuronal processes corresponding to areas indicated in *A* from CaNwt (*B*1 and *B*3) or CaNCA (*B*2 and *B*4) injected mice. Arrows indicated neurites or axons with typical dystrophies. (*C*–*D*) Images of dendritic spine (*C*) and quantitative analysis of spine densities (*D*) from live imaging of neurons without apparent dystrophies shows a decrease in spine density with CaNCA overexpression. In *C*, arrows indicated spines and arrow head

indicated neurites with typical dystrophies. *, $P < 0.05$; Values represent mean $\pm$ SD (n = 4 animals for each condition and total > 400 spines).
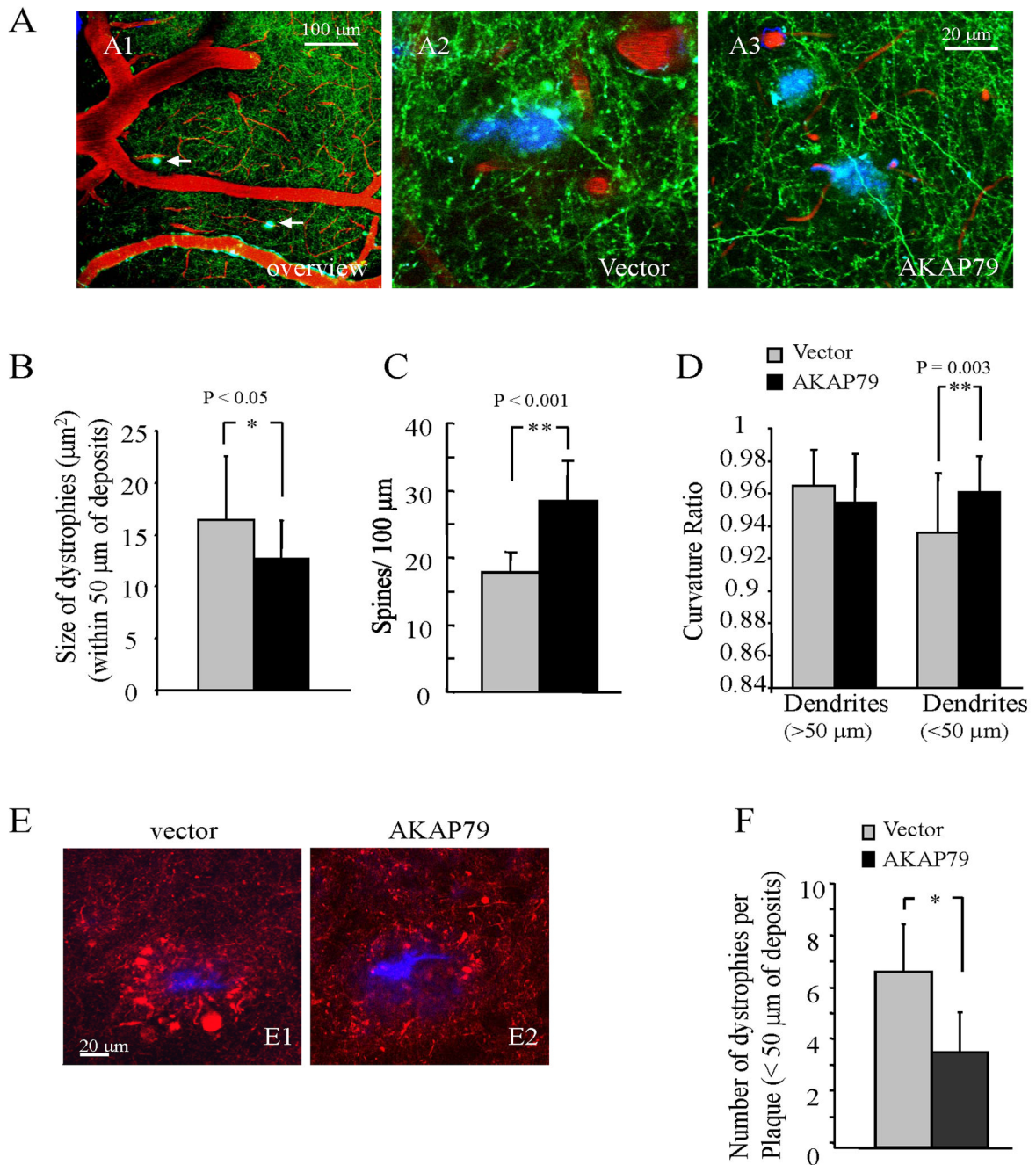
Figure 9.
Abnormal morphologies are prevented by overexpression of CaN inhibitory peptide AKAP79 in APP/PS1 mouse brain. (*A*1) *in vivo* low magnification image of GFP expressing neurites and axons (green), blood vessels containing Texas Red, and amyloid deposition stained with methoxy-XO4 (blue). Arrows indicated Aβ deposits. (*A*2 and *A*3) High magnification live images taken from around 100 µm below the brain surface in the neocortex of adult APP/PS1 mice show dendritic spines and dystrophies in both vector and AKAP79 expressing conditions. (*B–D*) Quantification of spine density (*B*), dendritic dystrophies (*C*) and neurite curvature (*D*) near Aβ deposits in vector or AKAP79 expressing APP/PS1 mouse brain shows that AKAP79 expression decreases dystrophy size (*B*, vector: 16.4 ± 6.1 µm2; AKAP79, 12.8 ±

3.6, p = 0.029, n = 45 from 4 animals), increases spine density (*C*, vector: 17.8 ± 3.0 / 100μm; AKAP79, 28.3 ± 6.1, p < 0.001, n > 400 spines), and decreases abnormal neurite curvature near plaques (*D*). (n = 4 animals for each condition and total > 400 spines). (*E*) Postmortem sections indicated axonal dystrophies with SMI312 staining (red) and plaques with thioflavine S (blue) shows that plaque-associated axonal dystrophies are reduced (quantified in f, vector: 16.4 ± 6.1 μm^2; AKAP79, 12.8 ± 3.6, p = 0.0291, n = 45 plaques from 4 animals) in areas injected with AKAP79. (*F*) Quantification of numbers of axonal dystrophies per single Aβ deposits from postmortem sections. Values represent mean ± SD *, *P* < 0.05; ** *P* < 0.01;